# Breaking Masked Implementations of the Clyde-Cipher by Means of Side-Channel Analysis

## A Report on the CHES Challenge Side-Channel Contest 2020

Aron Gohr[1], Friederike Laus[2] and Werner Schindler[2]

[1] Independent Researcher, Auckland, New Zealand aron.gohr@gmail.com
[2] Bundesamt für Sicherheit in der Informationstechnik (BSI), Bonn, Germany
firstname.lastname@bsi.bund.de

**Abstract.** In this paper we present our solution to the CHES Challenge 2020, the task of which it was to break masked hardware respective software implementations of the lightweight cipher Clyde by means of side-channel analysis. We target the secret cipher state after processing of the first $S$-box layer. Using the provided trace data we obtain a strongly biased posterior distribution for the secret-shared cipher state at the targeted point; this enables us to see exploitable biases even *before* the secret sharing based masking. These biases on the unshared state can be evaluated one $S$-box at a time and combined across traces, which enables us to recover likely key hypotheses $S$-box by $S$-box.

In order to see the shared cipher state, we employ a deep neural network similar to the one used by Gohr, Jacob and Schindler to solve the CHES 2018 AES challenge. We modify their architecture to predict the exact bit sequence of the secret-shared cipher state. We find that convergence of training on this task is unsatisfying with the standard encoding of the shared cipher state and therefore introduce a different encoding of the prediction target, which we call the *scattershot encoding*. In order to further investigate how exactly the scattershot encoding helps to solve the task at hand, we construct a simple synthetic task where convergence problems very similar to those we observed in our side-channel task appear with the naive target data encoding but disappear with the scattershot encoding.

We complete our analysis by showing results that we obtained with a "classical" method (as opposed to an AI-based method), namely the stochastic approach, that we generalize for this purpose first to the setting of shared keys. We show that the neural network draws on a much broader set of features, which may partially explain why the neural-network based approach massively outperforms the stochastic approach. On the other hand, the stochastic approach provides insights into properties of the implementation, in particular the observation that the $S$-boxes behave very different regarding the easiness respective hardness of their prediction.

**Keywords:** Lightweight cryptography · Clyde-cipher · Side-channel analysis · Countermeasures · Masking · Secret-sharing · ISW-Multiplication · Deep neural network · Residual neural network · Stochastic approach · CHES Challenge 2020

## 1 Introduction

Nowadays, there are several emerging areas such as the Internet of Things, healthcare, distributed control systems, sensor networks or cyber physical systems, in which highly-constrained devices are interconnected, typically communicating wirelessly with one another, and working in concert to accomplish some task. This poses new challenges to the cryptographic community, as these devices process more and more sensitive data while being themselves usually not very well protected and thus easily accessible. Furthermore, because the majority of current cryptographic algorithms was designed for desktop/server environments, many of these algorithms do not fit into constrained devices whose computational power is limited.

This raises the need for new cryptographic algorithms that on the one hand can be operated under limited resources and on the other hand can be protected against side-channel and fault attacks without loosing too much of its performance. It further served the National Institute of Standards and Technology (NIST) in August 2018 as motivation for a competition searching for so-called *lightweight* ciphers that fulfill the demands for efficiency and side-channel resistance mentioned above [19]. NIST received 57 submissions to be considered for standardization. After the initial review of the submissions, 56 were selected as Round 1 candidates, out of which 32 were selected to continue to round 2. On March 29, 2021, NIST announced ten finalists that are currently standardized.

One of the second round candidates is the *Spook* authenticated encryption scheme with associated data (AEAD) [4]. Its block cipher is the so called *Clyde* cipher that follows a tweakable LS-design consisting of 6 rounds. Clyde can efficiently be protected against side-channel attacks by Boolean masking and the aim of the CHES challenge 2020 was to examine the effectiveness of this countermeasure. For that purpose several challenges varying in the amount of masking were posted prior to the CHES conference 2020 [5]. A team of eight colleagues[1] at BSI worked on the software challenges and won all the prizes that were finally awarded.

**Main Contributions** In this paper, we provide a detailed description as well as a further analysis of our solution to the different challenges. Using a deep neural network, we were able to overcome the masking countermeasure by extracting a lot of information on the unmasked cipher state already from a single trace. This required seeing all bits of the masked internal state with very high bias, which proved difficult, since some bits of the internal state were much more challenging to learn for our neural networks than others. Indeed, our attempts to directly predict some of these bits seemed to not converge to results better than random guessing.

In order to achieve convergence for all bits of the targeted internal state variable, we represent the internal state in a way which is designed to achieve the following objectives:

- The chosen state representation allows for full and efficient reconstruction of the standard representation of the internal state as a bit-vector, even in the presence of noise (i.e. taking a target state $s \in \mathbb{F}_2^{128d}$ with alternative representation $v \in \mathbb{R}^n$, any $v' \in \mathbb{R}^n$ with small $\|v - v'\|_2$ should suffice to reconstruct $s$ without much error).
- The chosen state representation should make it difficult to reduce loss by making progress on the prediction of easy bits in isolation. Instead, progress on predicting any part of the target vector should be correlated with progress on the whole prediction problem.

We achieve this by a surprisingly simple method, namely by sending the target values through a *random linear map* before training. Given a list of training traces $X$ and a list of target internal state values $Y$, we hence essentially replace $y_i \in Y$ with $y'_i := Ay_i$, where multiplication is performed over $\mathbb{Z}$ and $A$ is a random binary matrix. We then try to learn to predict $y'_i$ from $x_i \in X$ by minimizing standard mean squared error loss. When using the trained model on new power traces, we simply multiply the model output with the Moore-Penrose pseudoinverse $A^+$ of $A$ to obtain predictions for each bit of the target state.

[1] Members of the BSI-team (in alphabetical order): Tobias Damm, Aron Gohr, Sven Jacob, Dominik Klein, Friederike Laus, Natalie Peter, Werner Schindler, Vivien Thiel.

We call this method of sending the target values that our model is intended to ultimately predict through a random linear function the *scattershot encoding*.

That a simple random transformation of the target values helps to obtain a better model is to some extent surprising, since a linear post-processing step of this type is in principle easy to represent for a neural network. This makes the scattershot encoding worthy to be studied on its own. We show that convergence problems similar to those observed with the side-channel task under consideration appear also in a synthetic problem, namely when trying to teach a neural network to compute a simple $\mathbb{F}_2$-linear function, and that the scattershot encoding helps achieve uniform convergence at that task as well.

Having obtained models for all of the software challenges of the CHES 2020 side-channel contest, we afterwards study their performance. We find that the easiest, 3-share challenge can be solved with around 20-30 traces, whereas a few ten thousand traces are required for the hardest 8-share challenge. Our analyses also reveal that different nibbles of the unshared internal state still represent vastly different levels of difficulty to our neural network, which is unexpected, since the implementation runs all nibbles in parallel using the same code.

Finally, we complete our findings by applying the stochastic approach as a "classical" statistical profiled method to the problem at hand. We find that our neural network and the stochastic approach consider the same parts of the internal state to be difficult to predict; however, the performance of the neural network is vastly superior. An further analysis of the leakage the two approaches exploit might serve as an explanation for this behavior, as it turns out that the AI-based approach is able to extract information from a much larger range of the trace.[2]

**Related Work** Deep learning recently entered the field of side-channel analysis and turned out to be a powerful tool that enlarges an attackers' capabilities compared to other techniques. For a recent overview on the subject we refer to [21] and the references therein. The neural network architecture used in our deep learning approach was first introduced in [11] to break a protected AES implementation. In [11], the side-channel attack extracted the Hamming weights of all AES subkeys. Afterwards, a equation solving stage was used to perform a limited amount of error correction on the extracted Hamming weights while simultaneously deriving the full key values from the Hamming weight guesses. This work uses the same network architecture, but cannot use any of the subsequent post-processing ideas used in [11]. There are multiple reasons for this: the Clyde-128 key schedule does not impose significant constraints on the values we might recover the side-channel data made available in the contest does not cover the full round number of the cipher anyway and we never get to see any unmasked internal state in the Clyde attack.

Our solution to the CHES challenge presented in this paper combines a signal extraction stage relying heavily on a neural network with classical elements, such as the choice of a suitable leakage target variable and leakage model as well as a manually designed key extraction stage that combines leakage over many traces to derive the target key.

In general, the question whether AI-based methods are superior over classical statistical methods is of great interest, and we complete our analysis of the strength of the neural network based leakage extraction stage by developing an alternative solution based on the stochastic approach. Combining classical and machine learning based techniques in order to achieve the best possible exploitation of the available signal is common in state-of-the-art side-channel attacks, since it is expected that some parts of optimal attacks will be difficult for neural networks to execute. Accordingly, there is a significant amount of recent research that is aimed at combining the strengths of deep learning and classical methods in side-channel analysis; for instance, a first approach that combines the stochastic

[2] The code for reproducing the results and experiments of our paper can be found at https://github.com/agohr/ches_ctf_2020.

approach with deep learning methods has recently been proposed in [25].
Another attack on the same data set as used in the present paper has been proposed in [6]. The authors essentially show that a template attack can reach an overall similar level of performance as our attack if it uses a deep understanding of the implementation. We show that results comparable to theirs can be achieved by a neural network based attack that exploits only the knowledge of the cipher state at one well-chosen point of the cipher's execution if a good representation of the training target is chosen.
Other notable recent work considered the possibility of combining classical template attacks with deep learning based preprocessing of input traces, achieving competitive results on several datasets at relatively low training cost [23].

**Outline** The outline of the remaining paper is as follows: First, we describe in Section 2 the side-channel contest of the CHES challenge 2020 before we detail the Clyde-128 cipher and its masked implementation in Section 3. Then, in Section 4 we present our solution to the CHES challenge based on a residual neural network and provide in Section 5 further insights gained with the stochastic approach. Finally, conclusions and an outline of future work are given in Section 6.

# 2 CHES Challenge 2020 Side-Channel Contest

## 2.1 Objectives

The CHES challenge 2020 [5] consisted in a side-channel contest whose objective it was to use side-channel analysis to break masked implementations of the Clyde-128 cipher [4]. The challenge involved a total of seven sub-challenges. Four of the challenges targeted a software implementation of Clyde-128 protected by an efficient variant of ISW-masking proposed by Goudarzi and Rivain [12] with 3, 4, 6 and 8 shares. The remaining three challenges targeted a hardware implementation of Clyde-128 using the glitch-resistant ISW-masking developed by Cassiers et al. [7]. This paper focuses completely on the software challenges. In the context of this contest, breaking an implementation means deriving from trace and tweak information a simple ranking of all possible keys such that the expected rank of the correct key is below $2^{32}$.

## 2.2 Data Sets and Evaluation Framework

For each challenge, the organizers collected and published large random- and fixed-key datasets. The random-key datasets for the software challenge consisted of 200,000 power traces covering the first half of the first round of the execution of Clyde-128 on the all-zero message block with varying tweak values; tweaks, keys and shared keys were also given. The fixed-key datasets contained only the trace and tweak information. Additionally, the organizers provided the source code of the corresponding implementations, proof-of-concept attacks on the weakest software and hardware targets, documentation explaining the main ideas behind the implementations and an evaluation environment based on the container tool singularity [17]. Submissions were tested against unknown test data held by the organizers.

# 3 Clyde-128 Cipher

In this section, we briefly describe the Clyde-128 cipher, before we detail its masked software implementation in the context of the CHES challenge 2020. The description of the cipher is based on [4], with slightly adapted notation, while the description of the masked implementation is based on code inspection.

## 3.1 TLS Design

The Clyde-128 cipher is a tweakable block cipher that is part of Spook, an algorithm for authenticated encryption with associated data (AEAD) and a second-round candidate of the NIST Lightweight Cryptography competition.[3] It relies on a tweakable LS-design (TLS-design) [14, 13] and works on $n = (s \cdot l)$-bit states, where $s = 4$ denotes the size of the $S$-box and $l = 32$ the size of the $L$-box. The full cipher state is referred to as $x \in \mathbb{F}_2^{s \times l}$, a row state is denoted as $x[i, \cdot]$, $i = 0, \dots, s-1$, and a column state as $x[\cdot, j]$, $j = 0, \dots, l-1$. In the following, we will simultaneously use bitmatrices $x \in \mathbb{F}_2^{s \times l}$ as well as row-wise reshaped bitvectors $B \in \mathbb{F}_2^{s \cdot l}$, which are related via

$$x[i, j] = B[i \cdot l + j].$$

We will at some places also use the notations $x_i$, $x_{i,j}$ etc. if single bits are concerned; it will, however, always be unambiguous from context to which notation we refer.
The basic TLS-design is summarized in Algorithm 1 and next, we describe the different building blocks in more details.

**Algorithm 1** Clyde-128 TLS-design with $s$-bit $S$-box and $2l$-bit $L$-box.

```
Input: plaintext $p \in \mathbb{F}_2^{s \times l}$, tweakey TK $\in \mathbb{F}_2^{s \times l}$, $s$-bit $S$-box $S$, $2l$-bit modified $L$-box
  $L'$, where $s = 4$ and $l = 32$.
Output: ciphertext matrix $x \in \mathbb{F}_2^{s \times l}$
$x \leftarrow p \oplus \mathrm{TK}(0)$
for $\sigma = 0, \dots, N_s - 1$ do
    for $\rho = 0, 1$ do
        $r = 2\sigma + \rho$
        for $j = 0, \dots, l-1$ do
            $x[\cdot, j] = S\big(x[\cdot, j]\big)$
        end for
        for $i = 0, \dots, \frac{s}{2} - 1$ do
            $\big(x[2i, \cdot], x[2i+1, \cdot]\big) = L'\big(x[2i, \cdot], x[2i+1, \cdot]\big)$
        end for
        $x[\cdot, 0] \leftarrow x[\cdot, 0] \oplus W(r)$
    end for
    $x \leftarrow x \oplus \mathrm{TK}(\sigma + 1)$
end for
```

**Tweakey** The tweakey scheduling algorithm for the $n$-bit key $k \in \mathbb{F}_2^n$ and the $n$-bit tweak $T \in \mathbb{F}_2^n$ reads as follows: First, the tweak is divided into $\frac{n}{2}$-bit halves $t_0$ and $t_1$, that is, $T = t_0 || t_1$. Then, the tweakey depends on the remainder of the round index $i$ by division by three as

$$\begin{aligned} \mathrm{TK}(3i) &= k \oplus (t_0 || t_1) \\ \mathrm{TK}(3i+1) &= k \oplus (t_0 \oplus t_1 || t_1) \\ \mathrm{TK}(3i+2) &= k \oplus (t_0 || t_0 \oplus t_1). \end{aligned}$$

***S*-Box** The 4-bit $S$-box is a variant of the $S$-box proposed in [3] and can efficiently be computed using four AND-gates and four XOR-gates as follows: Let $x \in \mathbb{F}_2^4$ be a 4-bit

[3] For further information, see https://csrc.nist.gov/projects/lightweight-cryptography

word, then $y = S(x)$ is given by

$$\begin{aligned}
y[1] &= \big(x[0] \odot x[1]\big) \oplus x[2],\\
y[0] &= \big(x[3] \odot x[0]\big) \oplus x[1],\\
y[3] &= \big(y[1] \odot x[3]\big) \oplus x[0],\\
y[2] &= \big(y[0] \odot y[1]\big) \oplus x[3].
\end{aligned}$$

In fact, the for-loop in lines 7-9 of Algorithm 1 for the computation of the $S$-box is not necessary, but for a full Clyde-state $x \in \mathbb{F}_2^{4\times 32}$, the $S$-box can be computed as

$$\begin{aligned}
y[1,\cdot] &= \big(x[0,\cdot] \odot x[1,\cdot]\big) \oplus x[2,\cdot],\\
y[0,\cdot] &= \big(x[3,\cdot] \odot x[0,\cdot]\big) \oplus x[1,\cdot],\\
y[3,\cdot] &= \big(y[1,\cdot] \odot x[3,\cdot]\big) \oplus x[0,\cdot],\\
y[2,\cdot] &= \big(y[0,\cdot] \odot y[1,\cdot]\big) \oplus x[3,\cdot].
\end{aligned}\tag{1}$$

**$L$-Box** The modified $L$-box $L'$ acts on pairs of 32-bit words $(x, y) \in \mathbb{F}_2^{32} \times \mathbb{F}_2^{32}$ as

$$(a, b) = L'(x, y) = \begin{pmatrix} \mathrm{circ}(\texttt{0xec045008}) \cdot x^{\mathrm{T}} \oplus \mathrm{circ}(\texttt{0x36000f60}) \cdot y^{\mathrm{T}} \\ \mathrm{circ}(\texttt{0x1b0007b0}) \cdot x^{\mathrm{T}} \oplus \mathrm{circ}(\texttt{0xec045008}) \cdot y^{\mathrm{T}} \end{pmatrix},$$

where $\mathrm{circ}(c)$ denotes a circulant matrix with first row $c$ in hexadecimal notation, so that $c = \sum_{i=0}^{31} c_i 2^i$ corresponds to the row vector $(c_0, \ldots, c_{31})$. The $L$-box can efficiently be implemented as well using six word-level (left) rotations and six 32-bit XORs per word:

$$\begin{aligned}
a &= x \oplus \mathrm{rot}(x, 12),\\
b &= y \oplus \mathrm{rot}(y, 12),\\
a &= a \oplus \mathrm{rot}(a, 3),\\
b &= b \oplus \mathrm{rot}(b, 3),\\
a &= a \oplus \mathrm{rot}(x, 17),\\
b &= b \oplus \mathrm{rot}(y, 17),\\
c &= a \oplus \mathrm{rot}(a, 31),\\
d &= b \oplus \mathrm{rot}(b, 31),\\
a &= a \oplus \mathrm{rot}(d, 26),\\
b &= b \oplus \mathrm{rot}(c, 25),\\
a &= a \oplus \mathrm{rot}(c, 15),\\
b &= b \oplus \mathrm{rot}(d, 15).
\end{aligned}\tag{2}$$

Also the $L$-box can be computed in parallel for the two row pairs $\big(x[0,\cdot], x[1,\cdot]\big)$ and $\big(x[2,\cdot], x[3,\cdot]\big)$.

**Round Constants** Finally, the round constants, which can be computed using a 4-bit LSFR, are given by four bits that are XORed with the first column of the Clyde-state. They read for the different rounds $r = 0, \ldots, 11$ as

| | | | | | | | |
|---|---|---|---|---|---|---|---|
| $r = 0$ | $(1,0,0,0)$ | $r = 1$ | $(0,1,0,0)$ | $r = 2$ | $(0,0,1,0)$ | $r = 3$ | $(0,0,0,1)$ |
| $r = 4$ | $(1,1,0,0)$ | $r = 5$ | $(0,1,1,0)$ | $r = 6$ | $(0,0,1,1)$ | $r = 7$ | $(1,1,0,1)$ |
| $r = 8$ | $(1,0,1,0)$ | $r = 9$ | $(0,1,0,1)$ | $r = 10$ | $(1,1,1,0)$ | $r = 11$ | $(0,1,1,1)$. |

## 3.2 Masked Implementation

In the context of the CHES challenge 2020, the implementation of the Clyde-128 cipher is masked according to [12] by decomposing a sensitive variable $x \in \mathbb{F}_2^{s \times l}$ into $d$ shares $(x_0, \dots, x_{d-1})$ such that

$$x = x_0 \oplus \cdots \oplus x_{d-1}.$$

In the sequel, we add the shares as a third dimension to the data and denote masked versions of a variable/operator with $\tilde{\cdot}$, e.g. $\tilde{x} \in \mathbb{F}_2^{s \times l \times d}$ denotes the masked version of $x \in \mathbb{F}_2^{s \times l}$ and for $(i, j) \in \{0, \dots, s-1\} \times \{0, \dots, l-1\}$ it holds [

$$x[i,j] = \bigoplus_{\ell=0}^{d-1} \tilde{x}[i,j,\ell].$$

The masked Clyde-128 algorithm is summarized in Algorithm 2.

**Algorithm 2** Masked Clyde-128 Algorithm.

```
1:  Input: plaintext $p \in \mathbb{F}_2^{s \times l}$, tweak $T \in \mathbb{F}_2^{s \times l}$, shared key $\tilde{k} \in \mathbb{F}_2^{s \times l \times d}$, masked $s$-bit $S$-box $\tilde{S}$, masked $2l$-bit modified $L$-box $\tilde{L}'$, where $s = 4$ and $l = 32$.
2:  Output: ciphertext matrix $x \in \mathbb{F}_2^{s \times l}$
3:  $\tilde{x} \leftarrow \tilde{k}$
4:  $\tilde{x}[\cdot,\cdot,0] \leftarrow \tilde{x}[\cdot,\cdot,0] \oplus T(0)$
5:  $\tilde{x}[\cdot,\cdot,0] \leftarrow \tilde{x}[\cdot,\cdot,0] \oplus p$
6:  for $\sigma = 0, \dots, 5$ do
7:      $\tilde{x} = \tilde{S}\big(\tilde{x}, \texttt{refresh} = 1\big)$
8:      $\tilde{x} = \tilde{L}'(\tilde{x})$
9:      $\tilde{x}[\cdot,0,0] \leftarrow \tilde{x}[\cdot,0,0] \oplus W(2\sigma)$
10:     $\tilde{x} = \tilde{S}\big(\tilde{x}, \texttt{refresh} = 0\big)$
11:     $\tilde{x} = \tilde{L}'(\tilde{x})$
12:     $\tilde{x}[\cdot,0,0] \leftarrow \tilde{x}[\cdot,0,0] \oplus W(2\sigma + 1)$
13:     $\tilde{x} = \tilde{x} \oplus \tilde{k}$
14:     $\tilde{x}[\cdot,\cdot,0] = \tilde{x}[\cdot,\cdot,0] \oplus T(\sigma + 1)$
15: end for
16: $x = \tilde{x}[\cdot,\cdot,0] \oplus \cdots \oplus \tilde{x}[\cdot,\cdot,d-1]$
```

The masked state $\tilde{x} \in \mathbb{F}_2^{s \times l \times d}$ is initialized with the shared key $\tilde{k} \in \mathbb{F}_2^{s \times l \times d}$ in line 3, before the tweak $T \in \mathbb{F}_2^{s \times l}$ and the plaintext $p \in \mathbb{F}_2^{s \times l}$ are added to the first share slice $\tilde{x}[\cdot,\cdot,0] \in \mathbb{F}_2^{s \times l}$ in lines 4 and 5 respectively. The masked $\tilde{S}$-box is implemented based on (1). For the multiplications (AND-gates), the ISW-multiplication algorithm [15] given in Algorithm 3 is used, while the additions (XOR-gates) are computed sharewise. During the first computation of the $\tilde{S}$-box in each of the six rounds, a mask refreshing of $y[1,\cdot]$ is performed according to Algorithm 4 as an additional countermeasure (line 7). For $d \in \{1,2,3\}$, the mask refreshing algorithm is used with $m = 1$, while for $d \in \{4, \dots, 8\}$, it is run twice, first with $m = 1$ and then with $m = 3$. The refreshing method has been proposed and further analyzed in [2, 1].

The linear $\tilde{L}$-box in line 8 is computed based on (2) in parallel for the different shares and the constant $W(r) \in \mathbb{F}_2^s$ is added to the first share slice $x[\cdot,0,0] \in \mathbb{F}_2^s$ in line 12. Then, in line 13 the key is added to the current state and next, in line 14 the tweak to the first slice of the shares. Finally, the unmasked output is obtained by XORing the different shares.

The recorded traces capture the first half of the first round of Algorithm 2. An exemplary trace is given for $d = 4$ shares in Figure 1, where the ISW-multiplication of the $\tilde{S}$-box, the mask refreshing as well as the $\tilde{L}'$-box computation are clearly visible.[4]

[4] Image taken from https://git-crypto.elen.ucl.ac.be/spook/masked_spook_sw.

**Algorithm 3** ISW-Multiplication Algorithm.

```
Input: $d$-shares $(a_0, \ldots, a_{d-1})$ of $a \in \mathbb{F}_2^l$ and $(b_0, \ldots, b_{d-1})$ of $b \in \mathbb{F}_2^l$
Output: $d$-share $(c_0, \ldots, c_{d-1})$ with $\bigoplus_{i=0}^{d-1} c_i = \left(\bigoplus_{i=0}^{d-1} a_i\right) \odot \left(\bigoplus_{i=0}^{d-1} b_i\right)$
for $i = 0, \ldots, d-1$ do
    $c_i \leftarrow a_i \odot b_i$
end for
for $i = 0, \ldots, d-1$ do
    for $j = i+1, \ldots, d-1$ do
        $r_{ij} \overset{R}{\in} \mathbb{F}_2^l$
        $r_{ji} \leftarrow (a_i \odot b_j) \oplus r_{ij}$
        $r_{ji} \leftarrow r_{ji} \oplus (a_j \odot b_i)$
        $c_i \leftarrow c_i \oplus r_{ij}$
        $c_j \leftarrow c_j \oplus r_{ji}$
    end for
end for
```

**Algorithm 4** Mask Refreshing.

```
Input: $d$-share $(a_0, \ldots, a_{d-1})$ of $a \in \mathbb{F}_2^l$ satisfying $a = a_0 \oplus \cdots \oplus a_{d-1}$, parameter $m$
Output: refreshed $d$-share $(a'_0, \ldots, a'_{d-1})$ of $a \in \mathbb{F}_2^l$ satisfying $a = a'_0 \oplus \cdots \oplus a'_{d-1}$
for $i = 0, \ldots, d-1$ do
    $r_i \overset{R}{\in} \mathbb{F}_2^l$
    $a_i \leftarrow a_i \oplus r_i$
    $a_{(i+m) \bmod d} \leftarrow a_{(i+m) \bmod d} \oplus r_i$
end for
```

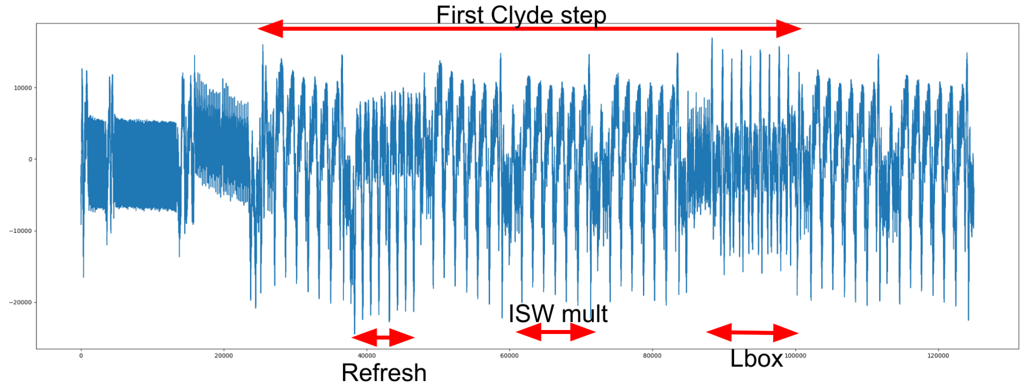

**Figure 1:** Exemplary trace for $d = 4$.

# 4 Deep Learning Approach

## 4.1 Overview

Our deep learning based solution to the CHES 2020 side-channel challenge relies on the following main ideas:

- We basically predict *Hamming weights* of some sensitive variables derived from the cipher state shares. To do so, we use a deep residual neural network following the architecture first introduced in [11].
- In the Hamming weight model, we actually derive many different but related sensitive variables from each state word via a technique that we call the *scattershot encoding*. In a nutshell, the intuition behind the scattershot encoding is to provide the neural network with a large number of interrelated tasks of varying difficulty that are close to the assumed leakage model (here: word-wise Hamming weight leakage of the shared cipher state) and which together solve the targeted prediction problem. For each trace, a prediction for the bit value of each shared cipher-state word can be derived from the predicted Hamming weights by applying the pseudoinverse of the scattershot encoding. Our findings indicate that these bit-level predictions are difficult or impossible to learn with the required precision for our network without the scattershot encoding.
- Finally, we combine bit-level predictions over many traces by predicting the unshared values of the sensitive variables. Comparing predictions from traces and key hypotheses, we get a ranking of the unshared keys.

In combination, these ideas allowed us to break all software challenges of the contest with much less data than was allowed in the contest. For instance, the 3-share challenge can be broken with $\approx 25$ traces.
In the sequel, we first describe our leakage target and the high-level strategy of our key recovery method. Our strategy presupposes that the shared cipher state at a particular point of execution leaks to the power trace essentially in its entirety, with only a modest amount of noise. This capability is achieved by combining a deep neural network with a simple post-processing step. Then we describe the structure of our deep neural network, the scattershot encoding, and how it is used to extract the shared cipher state at the target point.

## 4.2 Overall Strategy

**Targeted State** We target the cipher state after the first $S$-box. The unshared cipher state $x \in \mathbb{F}_2^{4\times 32}$ is given by $x = S(p \oplus T \oplus K)$, where $p \in \mathbb{F}_2^{4\times 32}$ denotes the plaintext, $T$ denotes the tweak value, and $S$ denotes application of the $S$-box layer. $S(p \oplus T \oplus K)$ depends in a simple way on plaintext, tweak and key and should therefore be well suited to constrain $K$ given partial knowledge of $S(\cdot)$ for several $p_i, T_i$. The fact that the $S$-box is involved means that errors in the key get spread out to 4 bits of the observed state, which should amplify the ability of the adversary to distinguish between almost-correct and fully correct key hypotheses. The dependence of the observed value on $p, T, K$ holds for each $S$-box separately, so that given successful recovery of the cipher state, a key ranking can be derived one $S$-box at a time, implying the ability to recover the whole key efficiently.

**Dealing With the Masking Countermeasure** Because of the presence of the masking countermeasure the cipher state is only available during execution in a secret-shared form. We will therefore try to read out the secret-shared cipher state $\tilde{x} \in \mathbb{F}_2^{4\times 32\times d}$ instead of

the unshared state. If we had the full shared state, the unshared state $x$ could be simply obtained by setting $x[a, b] = \oplus_{b=0}^{d-1} \tilde{x}[a, b, c]$.
Let $X$ be a random variable that is realized by a power trace reading and let $Y$ a random variable whose distribution coincides with that of the target states. Then, the image of $X$ is a subset of $\mathbb{R}^n$, where $n$ is the number of features in each power trace, $Y$ is uniformly distributed on $\mathbb{F}_2^{4\times d\times 32}$, and $X$ and $Y$ are dependent variables.
Assume that we possess an oracle $O$ which given a trace $t$ outputs values $p \in \mathbb{R}^{4\times d\times 32}$, where $p[a, b, c] \approx \mathbb{P}(Y[a, b, c] = 1|X = t)$, i.e. $p[a, b, c]$ approximates the probability that $\tilde{x}[a, b, c]$ is set given the information contained in the trace $t$. Then

$$\mathbb{P}(x[a, b] = 1|X = t) \approx \sum_{v\in M} \left( \prod_{0\leq i\leq d-1, v_i=1} p[a, b, i] \prod_{0\leq i\leq d-1, v_i=0} (1 - p[a, b, i]) \right),$$

where $M = \{v \in \mathbb{F}_2^d : v^t v = 1\}$.

*Remark* 1. Of course, $\{X = t\}$ is a zero set. In the above formula we tacitly assume that the conditional densities converge if we replace $t$ on the right-hand side by $\epsilon$-balls around $t$.

**Combining Leakage Across Traces** Let $\{t_0, t_1, t_2, \ldots, t_k\}$ be a set of traces with associated plaintexts $p_i$ and tweaks $T_i$. Given our oracle $O$, we can calculate for each $i$ and each $(a, c) \in \{0, 1, 2, 3\} \times \{0, 1, \ldots, 30, 31\}$ a probability $p_i[a, b] := O(t_i)$ for the corresponding bit value of the unshared target state to be set. We partition the key $K$ into 32 nibbles aligned with the $S$-boxes. Now, if $K[b] \in \mathbb{F}_2^4$ is a hypothesis for the $b$-th partial key, we calculate the true values $x[\cdot, b](K[b])$ given $p_i, T_i$ and $K[b]$. We consider the score $s(K[b])$

$$s(K[b]) := \left\| x[\cdot, b](K[b]) - p_i[\cdot, b] \right\|_2$$

and rank the key hypotheses in lowest-is-best order. Since $\|u_1 + u_2\|_2 = \|u_1\|_2 + \|u_2\|_2$ for orthogonal vectors $u_1, u_2$, adding up these partial key rankings for all indices $b$ is the same as using an analogous ranking method on the full key. We thus get a ranking of the full key space, where it is efficiently possible to determine the rank of any given key hypothesis up to a small error.

**Short Summary of Attack Workflow** In order to facilitate understanding, we give here a short summary of our attack workflow:

1. Input data: Power traces $T_0, T_1, T_2, ...$ for the implementation under attack.
2. For each $T_i$, do:
   (a) Use the neural network $Net$ to predict the scattershot encoding $E_i$ of the cipher state after the first $S$-box.
   (b) Derive predictions $b_{ij}$ for each bit of the state by reversing the scattershot encoding.
   (c) Derive a prediction $b_i$ for the unshared cipher state at the same point from these predictions.
   (d) Store the predictions $b_i$.
3. For each $S$-box, do:
   (a) For each key hypothesis, calculate the cipher state after the application of that $S$-box in the nibble of the state that the $S$-box is responsible for.
   (b) Rank the key hypothesis according to average distance of the predicted cipher state to the stored predictions derived from the power traces.
4. Output the best key hypotheses.

## 4.3 Deep Neural Network

In this subsection, we implement an oracle of the desired kind with the help of a deep neural network, whose output will be subject to a post-processing step to extract the shared cipher state. In particular, we give a rationale for our choice of neural network architecture, explain our training methods, and explain how the network outputs are transformed into predictions of the bits of the target variables.

**Leakage Model** In order to overcome the masking countermeasure, we need to obtain leakage on the exact value of the cipher state at some suitable point within the encryption operation. Early experiments showed that we could see the Hamming weights of the shared cipher state words very well. We therefore adopted a leakage model where every bit of the internal state leaks, although the leakage occurs possibly through Hamming weights of parts of the state instead of directly.

**Basic Ideas** Our deep residual neural network follows the architecture introduced in [11]. In particular, this entails the following:

- We treat Hamming weight prediction as a *regression problem and not as one of categorical prediction.* Simply put, our predictions are real-valued approximations of the integer values that represent the Hamming weights to be extracted. Compared to the interpretation of deep learning based side-channel analysis as a classification problem that is more popular in the literature on deep learning based side-channel analysis (see e.g. [24, 26] and the references cited therein), this has the advantage that the values we are trying to predict are in fact not categorical labels, but numbers.[5] By using a network that is a numerical regressor instead of a classifier, we can use that information to judge the severity of prediction errors, to alleviate the problem of rare output classes, and to induce an inductive bias towards mapping similar power traces to nearby Hamming weight estimates. In addition, we need numerical instead of categorical predictions for our post-processing of outputs using the pseudoinverse of the scattershot encoding.

- We treat the prediction problem as approximately *subsampling invariant.* This means that reducing the number of points in a trace might harm prediction accuracy, but should not introduce *systematic* errors in the predictions.

- A prediction of the sensitive variable produced by a relatively simple, shallow model may be improved upon by further post-processing.

On top of these ideas, the most important ingredient to the success of our deep learning model is that we create a very large number of mutually correlated prediction targets for the network. Together, these prediction targets solve the relatively difficult problem of predicting the value of the shared cipher state at a certain point of its operation with bit-level precision. For our model, we create a total of $400d$ prediction targets, where $d$ is the number of secret shares in the implementation under attack. These prediction targets can be broken down into $4d$ groups of targets, where each group contains one hundred targets that work together to solve one word of the shared state. Basically, the scattershot encoding transforms a bit-string into a sequence of Hamming weights of a large number

[5] It is a natural question *why* most of the literature on deep learning based side-channel analysis uses classification models instead of regression models, even when working in a Hamming weight leakage model, where this choice is theoretically expected to lead to suboptimal inductive biases. We conjecture that the main reason is the reuse of network architectures from the deep learning based image and audio *classification* literature; in addition, framing deep learning based side-channel analysis as a classification problem is a natural choice in power leakage models that seek to e.g. directly read out the value of some cipher state byte from power trace data.

of random sub-strings. Approximate knowledge of the Hamming weights of all of these substrings then yields approximate knowledge of all of the bits involved.
Since the resolution of the trace data and the number of state shares differs between the different software challenges, network parameters differ accordingly for the different challenges. Our neural networks are therefore parameterized by the following variables:

- *Input size $I$*: number of data points (equivalently, the size of the input layer) in each trace to be processed by the network.
- *Subsampling factor $q_1$* and *subsample size $q_2$*: number of subsampled versions of the input trace that are analyzed in parallel by the network as in [11] and the size of each subsampled trace. By definition, we have $I = q_1 \cdot q_2$.
- *Network depth*: number of residual blocks used by the network.
- *Word size $n$*: number of bits in each sensitive variable that we will try to extract from the traces. Generally, there will be $4d$ variables to extract for a challenge with $d$ secret shares.
- *Scattershot size $N$* and a set of *scattershot masks $m_1, m_2, \ldots, m_N \in \mathbb{F}_2^n$*: number of auxiliary sensitive variables that we generate in the scattershot encoding for each secret share and a randomly chosen generating set of $\mathbb{F}_2^n$.

For all four challenges we used a network depth of 10 residual blocks, a word size of 32, a scattershot size of 100 and a set of scattershot masks chosen at random once for all experiments. In contrast, $q_1$, $q_2$ and some training parameters needed to be chosen differently for different challenges; Table 1 gives details on all the challenges. Further details can be found in the supplementary data to this paper.

**Rationale for the Choice of Network** Our choice of neural network was motivated by the following considerations:

- Depending on the challenge, each trace consisted between 62,500 and 218,750 data points. In addition, we need to predict the entire shared cipher state at the attacked point in time; using a byte-level classifier (with 256 output units in the usual one-hot encoding), this would mean deriving 48 classifiers with 256 outputs each. Similar numbers of input and output features are reached in computer vision tasks (such as on multi-class semantic segmentation tasks like Cityscapes [8] or image classification tasks with a large number of classes such as ImageNet-1K [9]. However, the two-dimensional structure of the input data in these tasks makes it considerably easier for a convolutional neural network than in one-dimensional signal processing tasks to fuse information across the entire input sample. To the best of our knowledge, the only proposals for deep learning side-channel network architectures in the literature that are designed to process input traces with the resolution here under discussion are [18, 11]. The architectures proposed for instance in [16] process traces that are more than an order of magnitude smaller.
- The network architecture proposed in [18] uses deep implementation knowledge to set the field of view of the first convolutional block in the network. The network proposed in [11], on the contrary, reduces the dimensionality by a relatively implementation-agnostic splitting of the input trace into subtraces that only uses the assumption that the side-channel extraction task is subsampling invariant.
- Our initial study of the implementation suggested Hamming weight leakage; given that categorical predictors are theoretically expected to have some difficulties with

Hamming weight prediction due to class imbalance (see [20]) and loss of information about the output domain compared to a regression-based approach, the fact that the network proposed in [11] is a regressor is another point in its favour in this context.

- Our strategy to obtain bit-level predictions for the target state needs real-valued predictions of the Hamming weights. While it is possible to coax a classification model into producing such predictions by weighted-averaging of the prediction label values with weights given by the output activations, such a construction seems unnatural compared to simply using a regressor from the start.

In the following, we briefly describe each component of our neural network.

**Preprocessing** Given an input trace $T$ of size $I$, we first decompose the trace into subsampled traces $T_1, T_2, \ldots, T_{q_1}$, where $T_i$ consists of the points of $T$ with index $i \bmod q_1$. Each subsampled trace $T_i$ therefore contains $q_2$ points. The $T_i$ are subsequently called *slices* of the original trace.

**Number of Outputs, Output Activation** In total, our network generates $4Nd$ outputs for a $d$-share target. The ground truth associated to each output is the Hamming weight of some bit vector and therefore a priori a non-negative integer, making rectified linear units a natural choice for final layer activations, since they calculate a linear function of their input that is truncated to non-negative output values.

**The First Layer** After the preprocessing, each of the $q_1$ subsampled partial traces is processed first by a batch normalization layer. Each batch-normalized partial trace is then processed separately by a shared fully connected layer with $4Nd$ rectified linear outputs. The entire neural network state at this stage is thus comprised of $q_1$ vectors $v_i$ of $4Nd$ real values each, where $v_i$ is the vector associated to subsampled slice $i$. Each slice $v_i$ of the state is further subdivided into $4d$ *columns* of $N$ values. Each column of $N$ values is subsequently processed separately from the others (with communication only to the corresponding column in neighbouring slices of the overall network state) and intended to produce a prediction for the Hamming weights of the $N$ prediction targets corresponding to one 32-bit word of the shared state.

**Residual Blocks** Subsequently, each column is updated by repeating the following steps in a number of *residual blocks*, where each residual block computes the input of the next residual block:

1.) Batch normalize the current output state of each column.

2.) Apply a one-dimensional convolution of kernel size 3 with $N$ output channels to the batch normalized state of each column, running the convolution across all the slices after padding with zeros on both ends ("same" padding in Keras). Call the output vector of the convolution $(w_0, w_1, \ldots, w_{q_1-1})$.

3.) Add $v_i$ and $w_i$ together to obtain the input for the next residual block.

This structure is repeated for $t$ blocks, where $t = 10$ in all our experiments.

**Predicting the Target by Averaging** Finally, we are left with $q_1$ vectors $v_i \in \mathbb{R}^{4Nd}$ that we hope will approximate our prediction targets. These are subjected to a final averaging step that simply calculates the mean of the $q_1$ vectors and outputs it as our prediction.

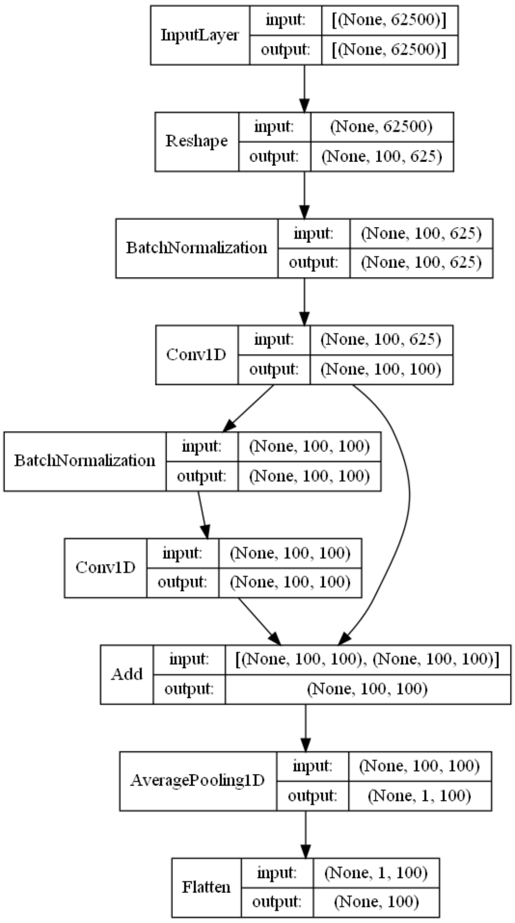

**Figure 2:** Visualization of one subnetwork of our neural network for the 3-share challenge, reduced to a single residual block. The entire network is composed of $d$ copies of this network. All of these $d$ copies share the same input (the input trace tensor), but are trained to predict the scattershot encoding of one particular cipher state word each.

**Schematic Overview of the Network Structure** To get an overview of the design of our network, Figure 2 shows the network design reduced to one residual block and the prediction of one cipher state word with the parameters relevant for the 3-share challenge. The 3-share network used to solve the challenge consisted of 12 copies of this network expanded to 10 residual blocks.

**Intuitions Behind this Architecture** This neural network architecture was first introduced for an AES side-channel task in [11], where it achieved highly precise byte-level Hamming weight prediction for all bytes of the expanded keys of a protected AES implementation. Here, splitting up the processing of the full trace into a number of subtraces helped to achieve dimensionality reduction, to reduce overfitting, and to leverage subsampling invariance of the side-channel prediction problem. The use of convolutional windows of width 3 allows some communication between the subnetworks processing different subsampled slices of the trace under consideration, which should improve slice-wise prediction quality. The choice of a deep residual neural network was motivated mainly by its good scaling with network depth.

**Possible Improvements to Our Network** While the design of the network we use addresses the issue of class imbalance to some extent by predicting the target Hamming weights it predicts as numerical values instead of as class labels, countermeasures against class imbalance such as those discussed in [20] would likely improve the prediction accuracy for rare classes. Likewise, we expect that additional regularization measures (for instance, regularization with noise or dropout as in [16]) would probably lead to more accurate predictions. However, since the main contribution of our solution – the scattershot encoding – is in Section 4.7 shown to have similar effects as in our problem in a simple synthetic data setting where perfect training data is freely available, it seems unlikely that these measures would solve the convergence problems observed in Figure 8. Finally, our solution might be improved by choosing a better network architecture or from manual points of interest (POI) selection. Designs that combine the subsampling invariance of [11] with a VGG-like architecture within each slice of the network could be promising candidates in this regard. We did not perform a thorough architecture search, since the design we chose based on our design rationale worked. We view the fact that no other entries were even submitted to the CHES 2020 CTF as evidence that other designs are not easily found by adapting proposals in the open literature.

A POI selection prior to any further processing, no matter how it is done, would lose subsampling invariance of the solution (because a fixed downsampling of the data is then being chosen). This means that any solution subsequently trained on the projected data would not be able to exploit subsampling invariance of the side-channel task; however, it is possible that this would be outweighed by the fact that removal of irrelevant points makes learning easier. One could consider adaptive POI selection, e.g. using an attention-like mechanism using a neural network. This would be advantageous over just using a neural network if the subsequent exploitation stage (i.e. the stage of a subsequent attack that uses the dimensionality-reduced representation of the input to obtain information on the target key) were able to perform some operation that neural networks do not learn well. On the other hand, it is in our point of view one of the main advantages of deep learning-based approaches that with suitable choices of training policy and network architecture, the network may learn on its own which parts of a trace are relevant and which are not. Indeed, one would usually hope that the network implicitly learns how to perform dimensionality reduction without losing much of the signal to be exploited, and this is a main design point in neural network architectures (ours included; the subsampling mechanism is directly a dimensionality reduction device not based on POI selection). Manual point selection, even if done by experts, will also run some risk of missing relevant points. We were for instance quite surprised when we found out that our trained networks apparently use parts of the trace where the $L$-box computation takes place (c.f. Section 5.3), which are not exploitable by "classical" statistical methods (such as templates or the stochastic approach; as opposed to neural network-based approaches) due to the huge number of shared key and masking bits that the evaluation of the $L$-box would require.

We leave all of these possible improvements to our architecture for future research.

## 4.4 The Scattershot Encoding: Achieving Bit-Level Precision

**Motivating Problem** In side-channel analysis, the adversary obtains usually only partial information about the target key by using the side-channel, but desires bit-level information, typically of some cryptographic key. They therefore will likely need to combine information from a large number of traces and/or use additional cryptanalytic techniques to determine the secret. For instance, in [11] first a neural network is used to approximately determine the Hamming weights of all bytes of the expanded AES key of the implementation under attack, and then a SAT solver subsequently computes the exact key from this partial information. Effectively, this strategy combines leakage from various parts of a single power trace with prior knowledge about the cipher under attack to exactly recover the key.

For the masked implementation of Clyde-128 under study in the CHES Challenge 2020, we were easily able to show significant leakage of the Hamming weights of the 32-bit words of secret-shared subkeys and cipher state at various points during the cipher's execution. However, each execution of the cipher uses fresh randomness for the computation of the initial secret sharing and the shares are refreshed with new randomness during the execution as well. This severely limits the ability of an adversary to combine leakage either across traces or across different leakage points within a single trace. Essentially, to find the secret key a significant amount of information about the *unshared* key must be exploitable from a single trace. This information can then be combined across traces to extract enough information on the unshared secret in order to enable an exhaustive attack on the remaining possibilities.

We tried to directly learn to predict single bits of the secret shares of the keys and cipher states. Our attempts, however, did not yield useful results even for the 3-share challenge, which is why we came up with the *scattershot encoding* that we detail next.

**Scattershot Encoding** Assume that we are given the task of guessing a bit string $b = b_1, b_2, \ldots, b_k$ and the only available information are the Hamming weights $h_i$ of $b \cdot m_i$, where $m_0, m_1, \ldots, m_l$ is a collection of known random bit strings of length $k$ and where $\cdot$ denotes component-wise multiplication. Once the $m_i$ form a generating subset of $\mathbb{R}^k$, this task is easy: assume without loss of generality that the $m_i$ form a basis, then

$$\sum_{j=1}^{k} m_i(j)\lambda_j = h_i$$

is a linear equation system with a coefficient matrix $M$ of full rank and $\lambda_i = b_i$ is its only solution. We call the weights $h_i$ the *scattershot encoding* of $b$ with respect to the masks $m_i$.

**Recovering Target Variables from Noisy Scattershot Encodings** In the presence of noise, recovering a bit string from its scattershot encoding with respect to a known set of masks becomes a problem of linear approximation in a natural way. Indeed, we can model the problem in an idealized setting as follows: assume that in the above situation we are given $\tilde{h}_i := h_i + X_i$ instead of the true encoding by the $h_i$ values, where the $X_i \sim N(0, \sigma^2)$ are i.i.d. normally-distributed random variables centered at zero. For a given combination of $\lambda_i \in \{0, 1\}$ to explain the observed $\tilde{h}_i$, we get $X = \tilde{h} - M\lambda$, where $X = (X_i)_{i=1,\ldots,k}$, $\tilde{h} = (\tilde{h}_i)_{i=1,\ldots,k}$. The probability density $p(\lambda)$ of $X$ at this value is (up to multiplicative, constant factor) given by

$$p(\lambda) \propto \mathrm{e}^{-\frac{\|\tilde{h} - M\lambda\|_2^2}{2\sigma^2}}.$$

If there is no prior knowledge about the true values of the $b_i$, sorting the candidates by descending value of $p(\lambda)$ yields an optimal guessing strategy in this situation. Since the exponential is strictly monotonously increasing irrespective of base (as long as the base is $> 1$), this ranking is the same as that obtained by ordering the values by $\|\tilde{h} - M\lambda\|_2$ in ascending order.

While it is possible to efficiently compute the ranking so induced (see e.g. [10]), it is in our context more useful to simply relax to the real numbers and find a minimal real solution for the $\lambda_i$ by linear regression. This is due to the fact that solutions to the relaxed problem contain some information on the amount of uncertainty about the value of specific bits $b_i$ of the sequence to be guessed, which is crucial for the implementation of our secret state oracle from the previous section. In addition, with a scattershot size of $N$, solving the linear regression can simply be done by multiplying the output array of the neural network for each share word from the right with a fixed $N \times 32$-matrix that only depends on the choice of scattershot masks.

**Table 1:** Challenge-specific parameters for our deep neural network.

| Challenge | Number of Epochs $N_e$ | Batch Size | Steps per Epoch | Validation Steps | $q_1$ | $q_2$ |
|---|---|---|---|---|---|---|
| Sw3 | 800 | 128 | 500 | 50 | 100 | 625 |
| Sw4 | 800 | 128 | 500 | 50 | 167 | 499 |
| Sw6 | 1000 | 32 | 2000 | 200 | 250 | 625 |
| Sw8 | 1000 | 32 | 2000 | 200 | 250 | 875 |

**Intuitions behind the Scattershot Encoding** We assumed that some kind of Hamming weight model would describe the leakage well, which was quickly confirmed by experiments. However, the question is which parts of the cipher state to calculate Hamming weights over: we were able to see word-level Hamming weights very well, but bit-level state recovery seemed significantly harder. In particular, achieving uniform convergence for all target bits of the shared state proved difficult in our experiments to recover the state bits directly. The scattershot encoding gives the neural network a number of different Hamming weight models to work with. In addition, all of these problems are highly correlated to each other, so progress on any of the scattershot targets should help the next layer in the deep residual network achieve better precision on all of the other targets. We hoped that with these assumptions, the scattershot encoding would help the network achieve faster and more uniform convergence across all target bits, which turned out to be true.

## 4.5 Training the Network

**Preprocessing the Data** To train our deep neural network, we first merged all of the released 10,000-trace random-key files from the competition website. This gave us a dataset of 200,000 traces with associated keys and tweaks, the plaintext being uniformly the zero message. We then computed a random shuffling of the training data and divided the shuffled data into a training and a validation set, holding out 20,000 traces for validation. We determined the cipher state based on the tweak, the secret-shared key and the plaintext data given in the original dataset using the Python implementation of the masked Clyde implementation provided by the organizers and subsequently brought it into scattershot encoded form by applying the relevant linear transformation. A set of scattershot masks was generated at random and can be found in the supplementary data set to this paper.

**Training** We generated minibatches for training and validation by random selection of samples from the training respectively validation set at training time using a generator, where we used different settings for the minibatch size for the different challenges. Likewise, the length of training (number of epochs and training steps per epoch, i.e. the number of minibatches used in each epoch) varied between the challenges.
For all training runs we used the Adam optimizer with a cyclic variable learning rate and mean squared error loss against the ground truth targets as loss function. At the end of each epoch, we calculated the mean squared error loss for the current network also on the validation set and stored the best network weights (according to validation loss) to disk. We set the learning rate $lr_i$ for epoch $i$ so that

$$\log_2(lr_i) = \log_2(\mathsf{low}) + \big(\log_2(\mathsf{high}) - \log_2(\mathsf{low})\big) \cdot \big((N_e - 1) - i \bmod N_e\big)/(N_e - 1),$$

where $N_e$ is the number of epochs in each cycle and $\mathsf{low}$ and $\mathsf{high}$ denote upper and lower bounds for the learning rates used in each cycle. In other words, each cycle used an exponential learning rate decay followed by resetting the learning rate to the *high* value at the beginning of the next learning rate cycle. We hoped that this setup would allow sufficient time for fine-tuning of weights at the lower learning rate levels as well as escape from local minima at the higher learning rates. We used $\mathsf{low} = 0.001$, $\mathsf{high} = 0.00002$ and $N_e = 10$ throughout our experiments. All relevant parameters are summarized in Table 1.

**Table 2:** Bitwise differences between the predicted and correct first word of secret-shared cipher state on Sw6. The first five traces of Rkey_Sw6_10000_19 served as test dataset. The model used in this experiment has been trained only on Rkey_Sw6_10000_0-14, so these examples were not seen by this model during training.

| Trace 1 | Trace 2 | Trace 3 | Trace 4 | Trace 5 |
|---|---|---|---|---|
| 0x81050d0 | 0x802e1810 | 0x5490 | 0x2015010 | 0x600142 |

**Computational Cost of Training** With network and training parameters as well as the sizes of input and output vectors of our networks being quite different between the different challenges, it is no surprise that the computational cost of training runs differs accordingly. For Sw3, a single training epoch using the parameters given in Table 1 takes about 100 seconds on a computer equipped with a single GTX 1080 Ti graphics card and a few gigabytes of not otherwise occupied RAM. A full training run can therefore be completed in about a day. For Sw8, on the other hand, a single epoch takes about 1050 seconds on the same machine, resulting in roughly a million seconds for a complete training run, or a bit less than two weeks.

## 4.6 Results

**Evaluation Data** Along with the random-key training data for each challenge, the organizers of the competition released fixed-key datasets to allow participants to evaluate the performance of their solutions. The fixed-key datasets were never used in either training or model selection, so results on these datasets should be representative of the performance reached for the key extraction task at hand.
In the sequel, we will have a closer look at the behavior of our solution on the simplest software challenge (Sw3, $d = 3$ shares). For the other challenges, we only report some statistics on whole-key ranking achieved with the appropriate number of traces.

**Single-Trace State Extraction** Our attack essentially first tries to match the observed traces to a probability distribution on the internal secret-shared cipher state. Then it computes the induced probability distribution on the corresponding unshared cipher state by calculating the convolution product of the $d$ share-distributions, compare equation (4.2), and finally matches the inferred distribution to all possible key hypotheses. For this to work well, we need fairly strong biases on the shared cipher state from a single trace, since the convolution product leads to a decay of any biases that is exponential in the number of shares.
Fortunately, we do get strong biases on the secret-shared state. Indeed, as Figure 3 shows, even some nibbles of the unshared key can be read out with high reliability already from a single trace in the Sw3 case. Interestingly, however, the results strongly depend on the considered $S$-box: some of them (e.g. $S$-box 17, but also $S$-boxes 23 and 26) seem to be rather easy to predict, while most $S$-boxes are harder (e.g. $S$-box 0), if not impossible to predict (e.g. $S$-boxes 16 or 21, whose key rank distribution is close to uniform).
This is even more apparent when we look at extracting the target secret-shared state after the first $S$-box layer. Table 2 shows some fairly representative examples of bitwise differences between predicted state and ground truth for a version of our Sw6 model trained on a slightly smaller data set than the model used in our attack on Sw6.

**Global Key Rank** We empirically determined the global key rank of our attack using the histogram-based method introduced by [10]. To do so, we performed 20 attack runs on randomly selected subsets of one fixed-key dataset provided by the organizers of the

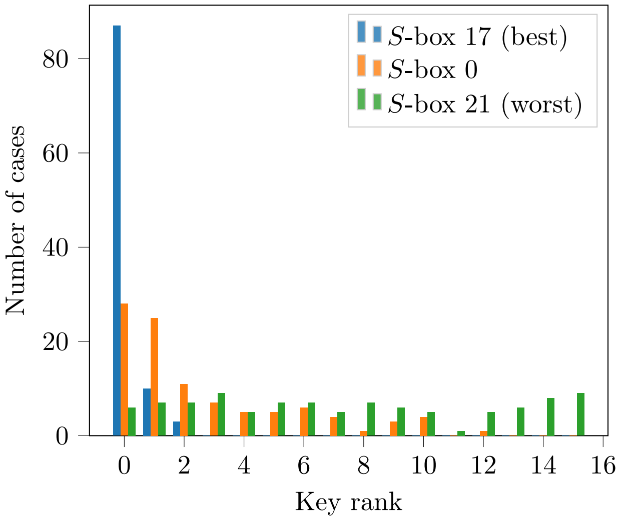

**Figure 3:** Key rank distribution in a single-trace attack for three selected $S$-boxes. For this test, 100 traces were selected at random from the Fkey_Sw3_K1_1000_0 data set and the key extraction algorithm was run separately on each trace. The statistic here shown gives the number of cases where the true partial key for the nibble in question was found at the rank given on the $x$-axis.

competition for each target; in general, the results we obtained were similar to those reported in the evaluation ("Hall of Fame") of the competition [5], for which according to the organizers five attack runs were performed. However, similar to [6], and different from the rules used in [5], we decided to evaluate our attack against the *median* key rank at a given number of traces; [5] used the *average* key rank. Since the key rank distribution has a very heavy tail, the average of the key rank of $n$ attack runs will generally be higher than the median of the key rank achieved in the same attack runs. This also makes it difficult to determine the mean key rank empirically, since a rare instance of very poor attack performance could still significantly change even an estimate that is based on a large number of tests.

Our attack requires about 20-30 traces to achieve a *mean* key rank below $2^{32}$ for 3 shares; about 200 for 4 shares; about 4,000 for the 6-share challenge; and about 70,000 for the 8-share challenge [5]. While especially the last figure is subject to much uncertainty, the numbers given by [5] do have the advantage that they were generated data that we never had access to. We do not know the corresponding numbers for the solution proposed in [6].

We also determined median key ranks for our solution. A detailed breakdown of our results for the different challenges can be found in Figure 4. We conjecture that the increase of the key ranks that can be observed at some points is due to the rather small sample size of only 20 attack runs.

**Table 3:** Number of traces that are needed to achieve a median key rank lower than $2^{32}$, comparison of our solution and [6].

| | Sw3 | Sw4 | Sw6 | Sw8 |
|---|---|---|---|---|
| This work | 25 | 105 | 3000 | 35000 |
| [6] | 50 | 120 | 1100 | 12000 |

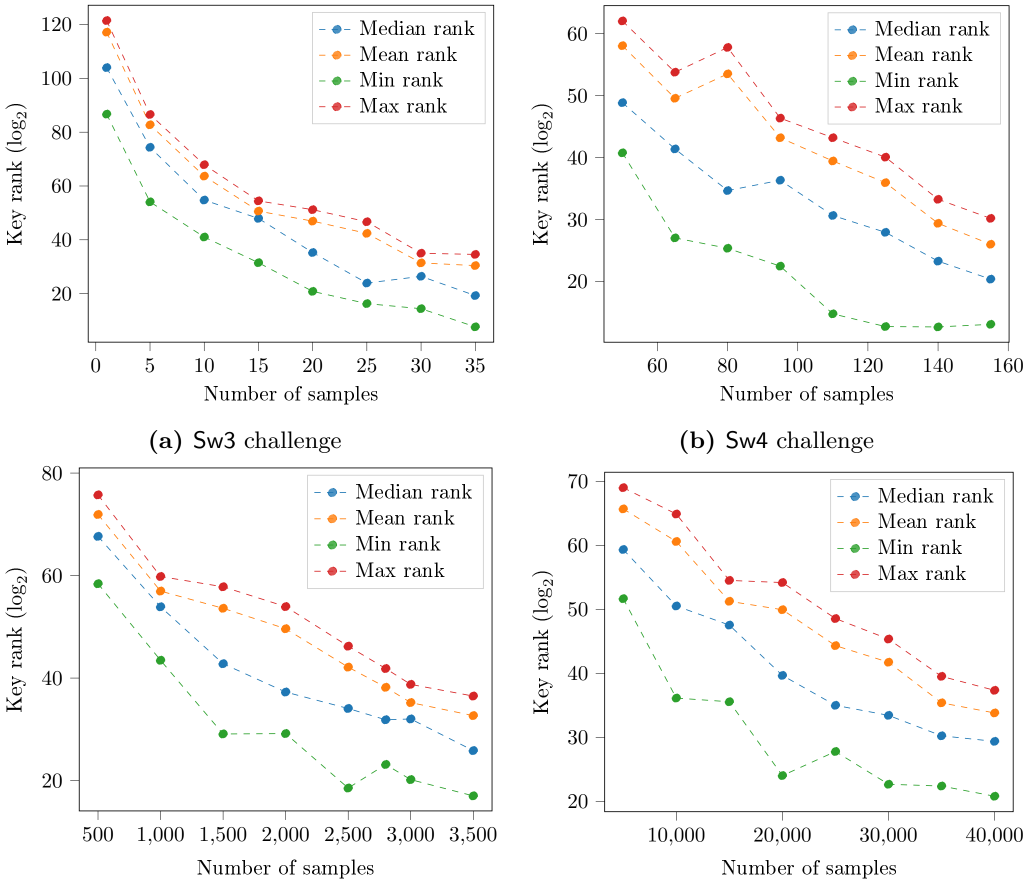

**(a)** Sw3 challenge

**(b)** Sw4 challenge

**(c)** Sw6 challenge

**(d)** Sw8 challenge

**Figure 4:** Key rank statistics for our solutions on the different software challenges. For each of the number of traces considered, 20 attacks were run against random subsets of the Fkey_Sw3_K2_1000_8 dataset (Sw3 challenge), the Fkey_Sw4_K0_1000_0 dataset (Sw4 challenge), the Fkey_Sw6_K0_10000_0 dataset (Sw6 challenge) respective all fixed key Fkey_Sw8_K0_x datasets taken together (Sw8 challenge).

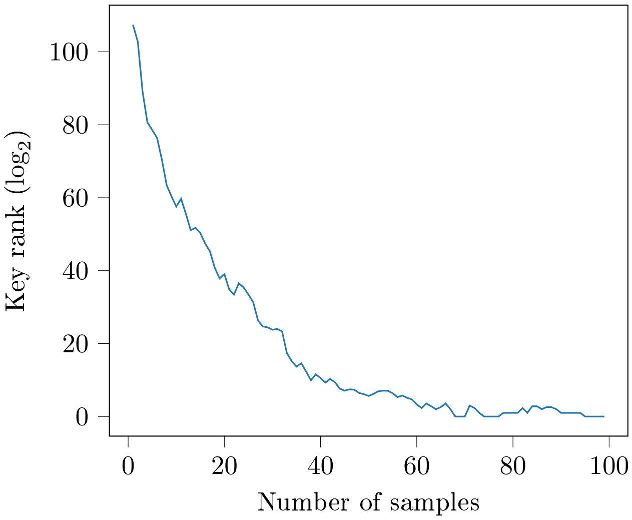

**Figure 5:** Key rank as a function of the number of samples used in an attack on the Fkey_Sw3_K0_100_0 data set. The figure shows the logarithmic key rank (base 2) obtained when using the first $n$ traces of the test set for key extraction, where the order of the samples is as in the original data set.

**Comparison to [6]** To the best of our knowledge, [6] is the only other published attack on the dataset of the CHES challenge. Their attack is not based on a neural network, but on a profiled Soft Analytical Side Channel Attack (SASCA). Their adversary uses a much deeper knowledge of the circuit to be attacked; this allows them to achieve superior performance on the 6-share and 8-share challenges, while falling short of our solution for the 3-share challenge. It is unclear how much of this advantage would remain after further optimization of both solutions; our network for the 8-share challenge had likely not plateaued yet after two weeks of training on a single GPU. On the whole, the two attacks reach a comparable level of performance in different ways, with the solution in [6] being inferior at low share numbers, but showing probably better asymptotic behavior. The number of traces required to reach a key rank less than $2^{32}$ is given in Table 3 for both solutions.

## 4.7 Dissecting the Scattershot Encoding

**Problem Statement** Our networks failed to learn the extraction of all output bits when we tried to learn to predict these bits directly. Instead, we predict a scattershot encoding of our target data. In the attack phase, we have to reverse the encoding in order to retrieve predictions for the bit-values of the shared target variables from the output of the network. This is surprising, since the scattershot encoding is nothing but a linear transformation of the output values. We therefore did some further investigations understand the success of this trick a bit better.

**Difficulties in Studying the Scattershot Encoding** The task under discussion in this paper makes it difficult to study problems in network convergence in a systematic way: even for the 3-share problem, the time to train an instance of our network is about a day on our hardware. Furthermore, it is difficult to say, in absolute terms, how well the obtained network exploits the available signal and to find out exactly which properties of the task cause the convergence problems.

**A Synthetic Problem** We therefore aimed at figuring out a simpler learning problem that would exhibit similar convergence problems as our side-channel task. To this end, we tried to learn the $\mathbb{F}_2$-linear function

$$f\colon \mathbb{F}_2^{32} \to \mathbb{F}_2^{32}, \quad f(x) = Ax,$$

where $A$ is the lower triangular matrix with all entries below or on the main diagonal equal to one. We tried to learn $f$ by observing random input-output pairs using a fully connected deep neural network.

*Remark* 2. The $i$-th coordinate function of $f$ is $f_i(x) = \bigoplus_{j=1}^{i} x_j$. The problem of learning the last of these coordinate functions in isolation (i.e. given only random inputs and $\{0,1\}$-valued outputs of the coordinate function) using feed-forward neural networks is expected to be difficult, which is confirmed by experiments: training feed-forward networks to predict the parity of 32-bit bitstrings fails unless the networks are trained with structured input. However, learning $f$ is expected to be easier, since the network is now forced to learn a number of XOR-sums. Some of these are of low Hamming weight and therefore easy to learn, and knowing how to compute these might be helpful for learning the components that are harder to predict.

**Neural Network Designs** In order to test the difficulty of learning to compute $f$ with and without the scattershot encoding, we considered two simple network architectures. Both of them are deep residual networks with ten residual blocks, where each block consists of a batch normalization layer followed by a fully connected layer with rectifier nonlinearities. They take a vector of 32 bits as input, have 100 nodes in each of the internal layers and use a single dense layer with ReLu activations after the input to expand the input to a vector of dimension 100. However, they differ in the output layers:

- The final layer of Model 1 uses a sigmoid activation function to obtain output values between 0 and 1 and outputs 32 such values, thereby directly predicting the target bits.
- Model 2 predicts a scattershot encoding of the target values and therefore outputs 100 values using a final linear activation.

**Training and Validation** Both models were trained for 100 epochs on the same training data set. Training was performed with the Adam optimizer using default parameters in Keras and a constant batch size of 5,000. Ten percent of the training set was withheld for validation in order to track the evolution of the loss value for both models.

**Testing** Finally, both models were tested using a freshly generated test set consisting of another $10^6$ example vectors. For each bit of the target output, we measured how often either prediction output matched ground truth.

**Results** Within the training budget of the experiment, Model 1 failed to converge on the last five bits of the target function; it predicted the other bits very well. Model 2, on the other hand, showed some degree of convergence for all bits, although the last two bits had accuracies of only 59 and 61 percent respectively when training was stopped. Figure 6 gives additional details.

Additionally, a qualitative comparison of the loss evolution for both models shows that Model 1 converges through punctuated equilibria, effectively learning to predict one bit of the target at a time and then getting stuck. The loss of Model 2, on the other hand, is smoothly decreasing throughout the training run. It is also worth noting that many of the equilibria require a temporary significant increase of validation loss to leave, suggesting

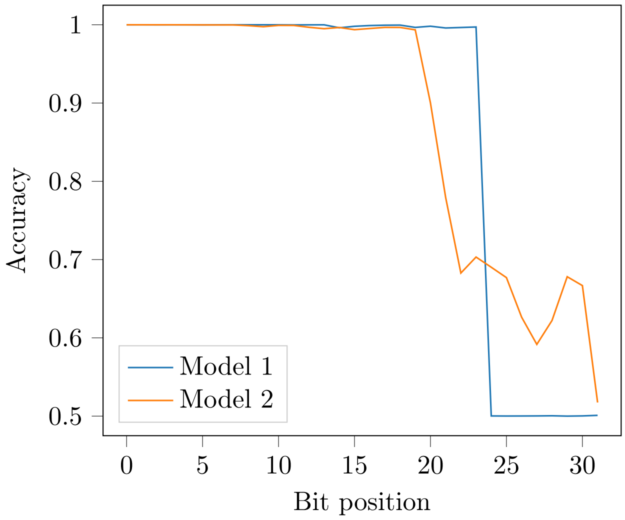

**Figure 6:** Accuracy of target prediction for Model 1 and Model 2 on learning a simple $\mathbb{F}_2$-linear function. The $x$-axis gives the targeted bit position inside the target and the $y$-axis shows the obtained accuracy. Model 2 uses a scattershot encoding of the targets, while Model 1 does not.

some stability of the corresponding local minima of the loss function. This is illustrated in Figure 7 which shows the validation loss progress of the mean squared error loss for Model 1 (left) and Model 2 (right) over 100 epochs of training. Note that the scale of the loss is not comparable between both approaches, since the range of the scattershot targets (which are Hamming weights of parts of the target vector) is much larger than the binary values of the target values themselves.

*Remark* 3. It is worth mentioning that our experiment described here using synthetic data contains no noise. In principle, there is no uncertainty about the signal and there is a simple algorithm that recovers all the target bits. Still, at least the results of the simple ML-based analysis we conducted suggest that some bits of the target are much less readily exploitable than others; the direct attack has difficulties to see any bias at all for some of them. It is tempting to speculate that the very strong differences we see in the apparent exploitability of different $S$-boxes in the CHES 2020 challenge task are likewise due partly or wholly to logical difficulties of extracting the signal instead of being due to the absence of an exploitable signal for the problematic $S$-boxes. This suspicion is (weakly) supported by the observation that the implementation provides no clear reason for the existence of these differences in leakage and the fact that the use of the scattershot encoding helps to solve some $S$-boxes that otherwise show no significant bias. The learning history of our direct attack attempt also showed some support for a pattern of temporary stalling over the first 400 epochs of training that is similar to that observed in the synthetic task, in spite of our use of a cyclic learning rate schedule to prevent the model from getting stuck in local minima (see Figure 8).

## 5 The Stochastic Approach

In this section we present further analyses and insights that we gained with the help of the stochastic approach [22]. We chose the stochastic approach for two reasons: Firstly, it is a very effective classical attack method against block ciphers, providing a serious

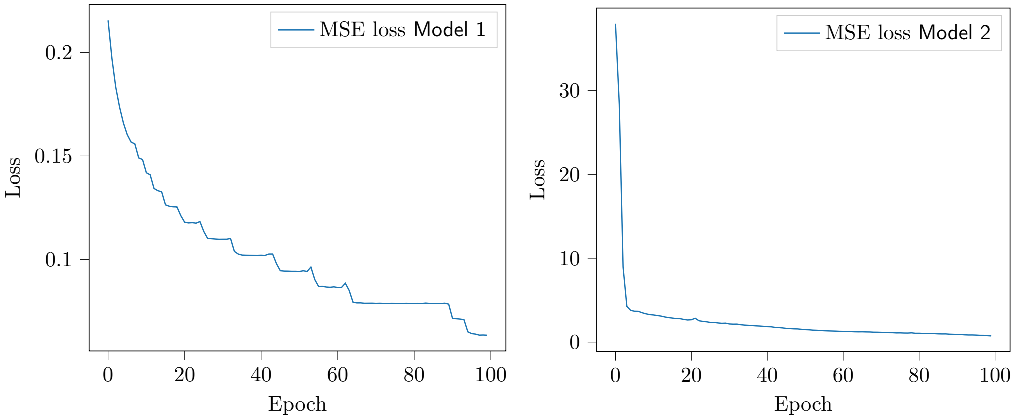

**Figure 7:** Validation loss evolution for Model 1 (left) and Model 2 (right) over 100 epochs of training.

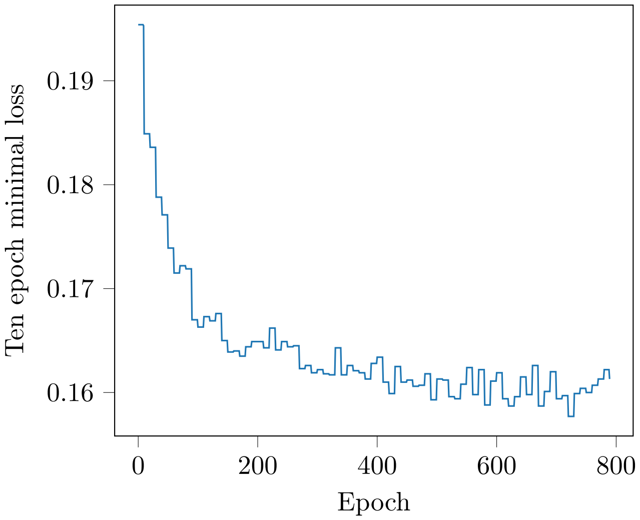

**Figure 8:** Development of the loss of our model in an attempt to directly learn predicting the target bits of the 3-share challenge. The loss given for each epoch is the lowest validation loss attained in the next ten epochs of training; this removes the effect of the cyclic learning rate schedule on loss development, which would otherwise clearly dominate. Some signs of capture by local minima are evident for epochs 60-87, 90-139 and 150-269.

benchmark for the neural network. Secondly, the stochastic approach allows insights into the properties of the leakage and thus of the targeted implementation.

To this aim, we extend in Subsection 5.1 the stochastic approach to a tweakable block cipher with shared keys whose implementation is protected by Boolean masking. After thorough analysis we show the results of some experiments (Subsection 5.2). Furthermore, we provide an explanation why some $S$-boxes are harder to attack than others. Finally, Subsection 5.3 contains a brief comparison between the attack efficiencies of the stochastic approach and of the neural network.

So far, the "standard" stochastic approach considers block ciphers with unshared keys, e.g., the AES cipher. It uses the stochastic representation

$$I_t(x, z, \tilde{k}) \coloneqq h_t(x, z, k) + R_t\,, \quad \text{(“standard” stochastic approach)} \tag{3}$$

which quantifies the random electrical current (or the power consumption) at time $t$, where its (unknown) distribution depends on the triple $(x, z, k)$. Here, $x \in \{0, 1\}^p$ denotes a part of the plaintext or ciphertext, $z \in M$ the masking bits, and finally $k$ denotes the subkey that is targeted by the attack. (Example: When attacking the AES, the subkey $k$ usually is a byte, and $p$ comprises one or two bytes, depending on whether the first or the last round is being attacked.) The *leakage function* $h_t(x, z, k)$ quantifies the deterministic part of the leakage (that depends on $(x, z, k)$) while the random variable $R_t$ models the noise. The noise summarizes the electrical current of operations that are computed in parallel to the targeted one (but are independent of $(x, z, k)$), and to some degree it may be affected by the power measurement. We assume that the noise vector $R_t$ is independent of $h_z(x, z, k)$ and normally distributed with expectation 0. The aim of the profiling phase is to estimate the joint distribution of the random current vector $\vec{I_t}(x, z, k)$ at several instants $t_1, \ldots, t_m$.

To handle the situation with shared keys we adjust the stochastic representation (3) in to

$$I_t(x, z, \tilde{k}) \coloneqq h_t(x, z, \tilde{k}) + R_t\,. \tag{4}$$

As can be seen, (4) is rather similar to (3), the main difference is that the subkey $k$ has been replaced by $\tilde{k}$, which denotes the part of the *shared key* targeted by the attack. Likewise, (4) quantifies the distribution of the random electrical current (or the power consumption) at time $t$, depending on the triple $(x, z, \tilde{k})$. Since we attack the execution of the Clyde cipher at its beginning, $x$ denotes a part of the plaintext (possibly including a tweak). Also here, $z$ denotes the masking bits, the leakage function $h_t(x, z, \tilde{k})$ quantifies the deterministic part of the leakage, and the random variable $R_t$ models the noise. As for block ciphers with unshared keys (3), the noise is caused by other operations (independent of $(x, z, \tilde{k})$) that are computed in parallel to the targeted one, and possibly affected by the power measurement. Again, we assume that the noise vector $R_t$ is independent of $h_z(x, z, \tilde{k})$ and normally distributed with expectation 0.

We will see in Subsection 5.1.3 profiling essentially works as in the "standard" case (with shared subkeys in place of subkeys), while for key extraction (attack phase) additional difficulties arise that require new strategies.

## 5.1 Different Steps of the Stochastic Approach

In this subsection we adjust the stochastic approach to shared keys. In particular, we develop two new decision rules for the key extraction phase.

### 5.1.1 Vector Space Bases for Different Substeps

The first task in the profiling phase is the estimation of the leakage function $h_t(x, z, \tilde{k})$ for each (potential) time point $t$ of interest, which can independently be done for each time $t$. The attacker/evaluator does not estimate the different function values $h_t(x, z, \tilde{k})$ (which would principally be possible but very inefficient), but the leakage function as a whole. In general, this works as follows: For each admissible shared subkey $\tilde{k}$ we define the restricted leakage function $h_{t;\tilde{k}}\colon \{0,1\}^p \times M \times \{\tilde{k}\} \to \mathbb{R}$, given by $h_{t;\tilde{k}}(x,z,\tilde{k}) := h_t(x,z,\tilde{k})$, which is essentially a function in $(x,z)$. We interpret $h_{t;\tilde{k}}$ as an element of the real vector space $\mathcal{F}_{t;\tilde{k}} = \{h'\colon \{0,1\}^p \times M \times \{\tilde{k}\} \to \mathbb{R}\}$. The aim is to define a suitable vector subspace $\mathcal{F}_{u,t;\tilde{k}}$ of $\mathcal{F}_{t;\tilde{k}}$, which is "close" to the unknown leakage function $h_{t;\tilde{k}}$, and to determine the best approximator $h^*_{t;\tilde{k}} \in \mathcal{F}_{u,t;\tilde{k}}$ of $h_{t;\tilde{k}}$ that has minimal $L^2$-distance.

The success of the stochastic approach depends on the choice of an appropriate vector space basis $g_{0,t;\tilde{k}}, \ldots, g_{u-1,t;\tilde{k}}$ of $\mathcal{F}_{u,t;\tilde{k}}$, together with suitable points of interest. To this aim it is necessary to identify and model the operations which are relevant for the current at a given time point. This requires a good understanding of the implementation and usually some trial and error, that means trying different points of interest and different vector space bases and observing which one fits best at the given time instance.

In this subsection we describe different operations of Algorithm 2 that can be used in the stochastic approach and provide the corresponding bases. To this aim, we fix an $S$-box $s$ and consider the different $S$-boxes separately.

(1) Key Loading (Line 3 of Algorithm 2), $4 \cdot d$ POIs
Assuming a Hamming weight leakage (see also Subsection 4.3), we can take the single bits of $\tilde{x}[\cdot, s, \cdot]$ as basis vectors, which are in total $4 \cdot d$ ones. This can be achieved if we set

$$h^*_t(\tilde{x}, z, \tilde{k}) := \beta_{0,t;\tilde{k}} + \sum_{i=0}^{3}\sum_{j=1}^{d}\beta_{i,j,t;\tilde{k}}\bar{g}_{i,j,t;\tilde{k}}(\tilde{x}, z, \tilde{k}),$$
$$g_{i,j,t;\tilde{k}}(\tilde{x}, z, \tilde{k}) = \tilde{k}[i, s, j-1].$$

(2) Tweak Addition (Line 4 of Algorithm 2), 4 POIs

$$h^*_t(\tilde{x}, z, \tilde{k}) = \beta_{0,t;\tilde{k}} + \sum_{i=0}^{3}\beta_{i,t,\tilde{k}}\bar{g}_{i,t;\tilde{k}}(\tilde{x}, z, \tilde{k}),$$
$$g_{i,t;\tilde{k}}(\tilde{x}, z, \tilde{k}) = \tilde{k}[i, s, 0] \oplus T[i, s].$$

(3) Computation of the $S$-Box (Line 7 of Algorithm 2), $d$ POIs
During the computation of the $S$-box there are according to (1) ISW-multiplications and XOR-operations that can be exploited. The evaluation of the $S$-box involves several masking bits in the thereby used ISW-multiplication, we first provide some further details on its evaluation, before we propose basis functions.

The $S$-box is applied to all shares of the $j^{th}$ column $\tilde{x}[\cdot, j, \cdot]$ of the working state, $j \in \{0, 1, \ldots, 31\}$. In the notation of (4) we have

- known plaintext $x = T(0)[\cdot, j] \oplus p[\cdot, j] \in \{0,1\}^4$, inclusive the tweak value; in the challenges $p[i,j] = 0$ for all $(i,j) \in \{0,1,2,3\} \times \{0,\ldots,31\}$. Formally, we may extend $x$ to the shares $1, \ldots, d-1$ by setting $x \equiv 0$ there, denoting this consistently by $\tilde{x}$.
- shared key $\tilde{K}[\cdot, j, \cdot] \in \{0,1\}^{4d}$ that is relevant for the $j^{th}$ $S$-box.
- masking bits: The evaluation of an $S$-box (1) requires four times Algorithm 3 (ISW-multiplication), four times an XOR-operation and once Algorithm 4 (mask refreshing). All together, these subalgorithms require $4\binom{d}{2} + 0 + d = 2d(d-1) + d = 2d(d - \frac{1}{2})$ masking bits.

In particular, $(x, z, \tilde{k}) \in \{0,1\}^4 \times \{0,1\}^{2d(d-\frac{1}{2})} \times \{0,1\}^{4d}$, and all the intermediate values that occur within the evaluation of the $S$-box can be expressed in terms of $x$, $z$ and $\tilde{k}$.

The amount of masking bits might become critical as it grows quadratically in the number of shares. Altogether, there are $2d(d-\frac{1}{2}) + 4d = 2d(d+\frac{3}{2})$ unknown bits (masking bits and shared key bits). This does not cause a problem in the profiling phase, but the key extraction (see Section 4) becomes numerically infeasible as the number of shares $d$ increases. For $d = 3$ the number of unknown bits equals 27, which should be feasible, but already for $d = 4$ it is 44.

Hence, at least for $d > 3$ strategies are needed that reduce the amount of unknown bits. All the shared key bits occur (implicitly) in the first two ISW-multiplications and in the subsequent XOR-additions (computing $y[1]$ and $y[0]$ for all shares). Mask refreshing is not relevant for these operations because it only updates $y[1]$ after it has been calculated. Restricting our attack on the $S$-box to these four substeps "wastes" the side-channel information which stems from the computation of $y[3]$ and $y[2]$. On the positive side this limits the number of unknown bits to $2\binom{d}{2} = d(d-1)$.

After these considerations, we exemplary show the proposed basis functions for the masked stated $\tilde{y}[1,:] = \underbrace{(\tilde{x}[0,:] \odot \tilde{x}[1,:])}_{=\tilde{q}} \oplus \tilde{x}[2,:]$. We always include $g_{0,t;\tilde{k}} = 1$ in our bases to model the (sub-)key-independent signal.

(a) (Single) ISW-Multiplication (Line 4 of Algorithm 3), $d$ POIs, masking bits $c_i = a_i \odot b_i$

$$h_t^*(\tilde{x}, z, \tilde{k}) = \beta_{0,t;\tilde{k}} + \sum_{j=1}^{d} \beta_{j,t,\tilde{k}} g_{j,t;\tilde{k}}(\tilde{x}, z, \tilde{k}),$$

$$g_{j,t;\tilde{k}}(\tilde{x}, z, \tilde{k}) = \tilde{x}[0,s,j-1]\tilde{x}[1,s,j-1].$$

(b) (Single) ISW-Multiplication (Lines 9 and 10 of Algorithm 3), $d(d-1)$ POIs $a_i \odot b_j$ and $a_j \odot b_i$, similarly as above

(c) (Single) XOR (according to (1)), $d$ POIs

$$h_t^*(\tilde{x}, z, \tilde{k}) = \beta_{0,t;\tilde{k}} + \sum_{j=1}^{d} \beta_{j,t;\tilde{k}} g_{j,t;\tilde{k}}(\tilde{x}, z, \tilde{k}),$$

$$g_{j,t;\tilde{k}}(\tilde{x}, z, \tilde{k}) = \tilde{q}[j-1] \oplus \tilde{x}[2,s,j-1].$$

In order to guarantee that the coefficients of the different basis vectors are of the same magnitude, we subtracted a global mean trace from all traces before computing the coefficients. (This significantly reduces the absolute values of the key-independent coefficients $\beta_{0,t;\tilde{k}}$, which would dominate otherwise, possibly spoiling the parameter estimation.) The remaining estimation of the basis coefficients $\beta_{j,t;\tilde{k}}$ can be performed as usual by solving a least-squares problem (with shared key bits in place of key bits).
The bases in (a), (b), and (c) are expressed in the sensitive variables that are operated at time $t$, and (in case of (b), in the masking bits) that are manipulated and by the targeted operation. The stochastic approach can be applied to these sensitive variables and masking bits, yielding the coefficients $\beta_{j,t;k}$. In a second step, after the estimation of the coefficients, the sensitive variables are expressed by $(x, z, \tilde{k})$. Note that the "direct" estimation of the function values $h_t(x, z, \tilde{k})$ would require $2^p|M|2^{4d}$ estimations per POI $t$. Instead, favoured by the Hamming weight based leakage model, the stochastic approach requires only a single least-square estimation.

*Remark* 4. (i) The real amount of masking bits depends on how far one evaluates computation of the $S$-box, e.g. whether one only considers $y[1]$, or $y[1]$ and $y[0]$, or the complete $S$-box. As mentioned earlier, using only $y[1]$ and $y[0]$ the masking bits needed for the mask refreshing of $y[1]$ can be neglected. On the negative side, some information gets lost.

(ii) Furthermore, the multiplications in the ISW-Algorithm 3 (line 4: $c_i = a_i \odot b_i$, line 9: $a_i \odot b_j$, line 10: $a_j \odot b_i$) can be observed *without* masking bits. As a consequence, the operations in (1), (2), (3)(a) and (3)(b) for $y[1]$ and $y[0]$ can be exploited completely without masking bits. Only the subsequent XOR in step (3)(c) that requires the execution of the full ISW-multiplication needs the masking bits $r_{ij}$ of the ISW-algorithm.

### 5.1.2 Estimation of the Covariance Matrix

The stochastic approach requires the estimation of a single covariance matrix to combine the information on the chosen points of interest $t_1 < \ldots < t_m$, which is quantified by the leakage functions $h_{t_1}, \ldots, h_{t_m}$. As mentioned earlier, we assume $R_t = I_t(x, z, \tilde{k}) - h_t(x, z, \tilde{k})$ to be centered normally distributed, and further that the $m$-dimensional random vector $(I_{t_1}(x, z, \tilde{k}) - h_{t_1}(x, z, \tilde{k}), \ldots, I_{t_m}(x, z, \tilde{k}) - h_{t_m}(x, z, \tilde{k}))$ is centered normally distributed as well for some covariance matrix $C$. Then

$$\vec{I_{\vec{t}}}(x, z, \tilde{k}) := \left(I_{t_1}(x, z, \tilde{k}), \ldots, I_{t_m}(x, z, \tilde{k})\right)$$

has $m$-dimensional density

$$f_{x,z,\tilde{k}} \colon \mathbb{R}^m \to \mathbb{R}, \quad f_{x,z,\tilde{k}}(\vec{i_{\vec{t}}}) = \frac{1}{(2\pi)^{m/2}\sqrt{\det C}} \mathrm{e}^{-0.5(\vec{i}_{\vec{t}} - \vec{h}_{\vec{t}}(x,z,\tilde{k}))^T C^{-1} (\vec{i}_{\vec{t}} - \vec{h}_{\vec{t}}(x,z,\tilde{k}))}. \tag{5}$$

Here, $\vec{t} = (t_1, \ldots, t_m)^T$ denotes the collection of points of interest and $\vec{i}_{\vec{t}}$ refers to the measured current vector at the time instances $t_1, \ldots, t_m$.
Since the exact leakage function $\vec{h}_{\vec{t}}$ ($m$-dimensional vector) is unknown in the key extraction phase, we substitute in (5) the estimated approximate leakage function $\tilde{\vec{h}}^*_{\vec{t}}$ and the estimated covariance matrix $\tilde{C}$, yielding the estimated density $\tilde{f}_{x,z,\tilde{k}} \colon \mathbb{R}^m \to \mathbb{R}$.

### 5.1.3 Key Extraction

The decision rule from the "standard" stochastic approach cannot be applied to shared keys. In Subsection 5.1.3 we develop, analyze and illustrate two decision rules for the key extraction in the presence of shared keys.
To better highlight the differences we briefly recall how the key extraction is done in the "standard" case: To this aim, let $\tilde{f}_{(st)x,z',k}$ denote the estimated density that corresponds to the triple $(x, z', k)$, where $k$ denotes an unshared subkey. The attacker decides for the subkey candidate $k'$ that maximizes likelihood function

$$\alpha_{(st)N_3}(k') := \prod_{j=1}^{N_3} \sum_{z' \in M} \tilde{f}_{(st)x,z',k'}(\vec{i}_{j;\vec{t}}) \tag{6}$$

(maximum likelihood estimator), where $\vec{i}_{j;\vec{t}}$ denotes the current vector of the $j^{th}$ power trace. As usual, all masking values are assumed to occur with the same probability.
Shared keys cause an additional difficulty: Although the unshared (sub)key is the same in all attack traces, the shared keys (which affect the leakage) are not. Let $\tilde{k} = (\tilde{k}_0, \ldots, \tilde{k}_{d-1}) \in \{0,1\}^{4d}$ be the targeted part of the shared key, while its $d$ components denote the 4-bit subvectors of the particular shares. Since for each power trace the key shares are selected

randomly they are in general different for all power traces. However, it is not necessary to determine all these subkey shares. Instead, it suffices to guess the (unshared) subkey $k \in \{0,1\}^4$ on the basis of $N_3$ power traces.
We introduce the subkey classes

$$\mathcal{C}(k') \coloneqq \{\tilde{k}' \coloneqq (\tilde{k}'_0, \ldots, \tilde{k}'_{d-1}) \mid \tilde{k}'_0 \oplus \cdots \oplus \tilde{k}'_{d-1} = k'\} \quad \text{for } k' \in \{0,1\}^4,$$

that means $\mathcal{C}(k')$ denotes the set of all shared key candidates for the slice $\tilde{K}[\cdot, i, \cdot]$ whose XOR-sum equals $k'$. Each class $\mathcal{C}(k')$ contains $2^{4(d-1)}$ elements because the shares $\tilde{k}'_0, \ldots, \tilde{k}'_{d-2}$ may attain any values while $\tilde{k}'_{d-1}$ is determined via $\tilde{k}'_{d-1} = k' \oplus \tilde{k}'_0 \oplus \cdots \oplus \tilde{k}'_{d-2}$.
We define the likelihood function $\alpha(\cdot)$ by

$$\alpha_{N_3}(k') \coloneqq \prod_{j=1}^{N_3} \sum_{\tilde{k}' \in \mathcal{C}(k')} \sum_{z' \in M} \tilde{f}_{x,z',\tilde{k}'}(\vec{i}_{j;\vec{t}}) \quad \text{for } k' \in \{0,1\}^4, \tag{7}$$

where $\vec{i}_{j;\vec{t}}$ denotes the current vector of the $j^{th}$ power trace. We decide for that key candidate $k^* \in \{0,1\}^4$, for which $\alpha_{N_3}(k^*)$ is maximal (maximum likelihood estimator). If the power consumption at the considered time instants $t_1, \ldots, t_m$ does not depend on all masking bits (e.g. because only one or two ISW-multiplications are considered), the inner sum in (7) has less than $2^{2d(d-\frac{1}{2})}$ terms, speeding up the evaluation of (7).

*Remark* 5. Depending on the number $m$ of points of interest it may be profitable to apply e.g. a PCA or LDA. This does not affect formula (7) in general, but only the densities $\tilde{f}_{x,z,\tilde{k}}(\cdot)$.

**Background and Justification of Decision Rule (7) and an Alternative Decision Rule**
For masked implementations with "usual" (i.e., unshared) keys the decision rule (6) is optimal (maximum likelihood estimate). For implementations with shared keys the situation is less clear. Although decision rule (7) appears to be a natural generalization, it deserves further explanations and a deeper analysis.
We assume that the relevant (targeted) parts of the plaintexts $x_1, \ldots, x_{N_3}$ and masking values $z_1, \ldots, z_{N_3}$ of the power traces $j = 1, 2, \ldots, N_3$ are realizations of independent and identically distributed random vectors $(X_1, Z_1), \ldots, (X_{N_3}, Z_{N_3})$. Since the tweak values are uniformly distributed, the $X_j$ can be assumed to be uniformly distributed on their domain as well. The random vector $\vec{I}_{\vec{t}}(X_j, Z_j, \tilde{k}_j)$ describes the $j^{th}$ random $m$-dimensional current vector at the time instants $\vec{t} = (t_1, \ldots, t_m)$, while $\tilde{k}_j \in \{0,1\}^{4d}$ denotes the correct shared subkey of trace $j$.
Assume that the random variables $X$ and $Z$ are independent and uniformly distributed on their respective domains. Then the random variable

$$f_{x,z';\tilde{k}'}(\vec{I}_{\vec{t}}(x, z, \tilde{k}))$$

quantifies the random $m$-dimensional density of a power trace for the shared key candidate $\tilde{k}'$ when $\tilde{k}$ is the correct shared subkey. At this point, $z$ denotes the correct masking value, while $z' \in M$ is an admissible masking value. We define

$$\begin{aligned} A(k' \mid k) &\coloneqq \sum_{\tilde{k}' \in \mathcal{C}(k')} \sum_{\tilde{k} \in \mathcal{C}(k)} \sum_{x \in \{0,1\}^p} \sum_{z \in M} \sum_{z' \in M} E_{\vec{R}_{\vec{t}}} \left( f_{x,z';\tilde{k}'} \left( \vec{I}_{\vec{t}}(x, z, \tilde{k}) \right) \right) = \\ &= 2^p |M| \sum_{\tilde{k}' \in \mathcal{C}(k')} \sum_{\tilde{k} \in \mathcal{C}(k)} \sum_{z' \in M} E_{X,Z,\vec{R}_{\vec{t}}} \left( f_{X,z';\tilde{k}'} \left( \vec{I}_{\vec{t}}(X, Z, \tilde{k}) \right) \right) \quad \text{for } k, k' \in \{0,1\}^4 \end{aligned} \tag{8}$$

Here, $E_{\vec{R}_{\vec{t}}}(\cdot)$ and $E_{X,Z,\vec{R}_{\vec{t}}}(\cdot)$ denote the expectation with respect to $\vec{R}_{\vec{t}}$ or $X, Z, \vec{R}_{\vec{t}}$, respectively. Since the shared subkeys are selected uniformly within the particular subkey classes, the term (8) equals (up to a constant) the expected value of $f_{x,z';\tilde{k}'}\left(\vec{I}_{\vec{t}}(x,z,\tilde{k})\right)$, averaged over randomly selected shared subkeys $\widetilde{k}' \in \mathcal{C}(k')$, $\widetilde{k} \in \mathcal{C}(k)$, random plaintexts $X$, random masking value $Z$ and admissible masking values $Z'$.

Recall that the random vectors $(X_1, Z_1), \ldots, (X_{N_3}, Z_{N_3})$ and the selection of the shared subkeys are assumed to be independent for all traces. Thus, to decide whether decision rule (7) can be successful it suffices to focus on the expectation of a single trace. Thus, if

$$A(k \mid k) > A(k' \mid k) \quad \text{for all } k, k' \in \{0,1\}^4, \tag{9}$$

the decision rule (7) finds the correct key (with large probability), provided that the sample size $N_3$ is sufficiently large. In other words, (9) provides a sufficient condition for the success of decision rule (7). At this point, note that if $Y$ denotes a $\mathbb{R}^n$-valued random variable with Lebesgue density $f(\cdot)$ and $g\colon \mathbb{R}^n \to \mathbb{R}$, then $E(g(Y)) = \int_{\mathbb{R}^n} g(y)f(y)\,\mathrm{d}y$ (provided that the integral exists).

Usually, decision rule (7) should be successful because the correct shared subkey $\tilde{k}$ should always provide a large contribution to the outer sum of (7) for the correct subkey class $\mathcal{C}(k)$. It is yet conceivable, depending on the leakage model of the targeted implementation, that within some wrong subkey class $\mathcal{C}(k'')$ several wrong shared key candidates give significant contributions to the corresponding outer sum, in total exceeding the sum for the correct subkey class $\mathcal{C}(k)$. If this happens it is necessary to develop an alternative decision rule to (7). A reasonable option would be to define the likelihood function $\alpha^*(\cdot)$ by

$$\alpha^*_{N_3}(k') := \prod_{j=1}^{N_3} \max_{\tilde{k}' \in \mathcal{C}(k')} \left\{ \sum_{z \in M} \tilde{f}_{x,z,\tilde{k}'}(\vec{i}_{j;\vec{t}}) \right\} \quad \text{for } k' \in \{0,1\}^4, \tag{10}$$

and to decide for that subkey candidate $k^* \in \{0,1\}^4$ for which $\alpha^*_{N_3}(k^*)$ is maximal (maximum likelihood estimator). For decision rule (10), the equivalent to (8) reads as

$$A^*(k' \mid k) := \sum_{\tilde{k} \in \mathcal{C}_k} \sum_{x \in \{0,1\}^p} \sum_{z \in M} \max_{\tilde{k}' \in \mathcal{C}(k')} \left\{ \sum_{z' \in M} E_{\vec{R}_{\vec{t}}}\left( f_{x,z';\tilde{k}'}\left(\vec{I}_{\vec{t}}(x,z,\tilde{k})\right)\right) \right\} \text{for } k, k' \in \{0,1\}^4.$$

The equivalent of the sufficient condition (9) is given by

$$A^*(k \mid k) > A^*(k' \mid k) \quad \text{for all } k, k' \in \{0,1\}^4. \tag{11}$$

**Example 1.** In this example we compute the terms $A(k' \mid k)$ and $A^*(k' \mid k)$. To keep the computations simple we consider 1-bit subkeys instead of 4-bit subkeys as above. We assume a non-masked implementation with leakage model $h_t(\tilde{x}, \tilde{k}) = a + b \cdot \operatorname{ham}(\tilde{x} \oplus \tilde{k})$. Here, $\tilde{x}, \tilde{k} \in \{0,1\}^d$, $a \geq 0$ and $b > 0$ are constants, while $\operatorname{ham}(\cdot)$ denotes the Hamming weight. In this scenario, only two subkey classes $\mathcal{C}(0)$ and $\mathcal{C}(1)$ exist, where

$$\mathcal{C}(i) = \left\{ \tilde{k}' = (\tilde{k}'_0, \ldots, \tilde{k}'_{d-1}) \mid \bigoplus_{j=0}^{d-1} \tilde{k}'_j = i \right\}.$$

We focus on a single time point $t$ (i.e., $m = 1$) and assume that the leakage $R_t$ is $N(0, \sigma^2)$-distributed. Since the implementation is not masked, the two inner sums (over $z$ and $z'$)

in the first line of (8) vanish. We compute the expectation

$$
\begin{aligned}
&E_{R_t}\left(f_{\tilde{x};\tilde{k}'}\left(\vec{I_{\vec{t}}}(\tilde{x},\tilde{k})\right)\right) = \int_{-\infty}^{\infty} f_{\tilde{x};\tilde{k}'}(y) f_{\tilde{x};\tilde{k}}(y)\,\mathrm{d}y \\
&= \frac{1}{\sqrt{2\pi}\sigma}\int_{-\infty}^{\infty} \mathrm{e}^{-\frac{\left(y-(a+\mathrm{ham}(\tilde{x}\oplus\tilde{k}')b)\right)^2}{2\sigma^2}} \frac{\mathrm{e}^{-\frac{(y-(a+\mathrm{ham}(\tilde{x}\oplus\tilde{k})b))^2}{2\sigma^2}}}{\sqrt{2\pi}\sigma}\,\mathrm{d}y \\
&= \frac{1}{\sqrt{2\pi}\sigma\sqrt{2\pi}\sigma}\int_{-\infty}^{\infty} \mathrm{e}^{-\frac{2y^2-2y(a+\mathrm{ham}(\tilde{x}\oplus\tilde{k}')b)-2y(a+\mathrm{ham}(\tilde{x}\oplus\tilde{k})b)+(a+\mathrm{ham}(\tilde{x}\oplus\tilde{k}')b)^2+(a+\mathrm{ham}(\tilde{x}\oplus\tilde{k})b)^2}{2\sigma^2}}\,\mathrm{d}y \\
&= \frac{1}{2\sqrt{\pi}\sigma}\frac{1}{\sqrt{2\pi}\frac{\sigma}{\sqrt{2}}}\int_{-\infty}^{\infty} \mathrm{e}^{-\frac{\left(y-\frac{(a+\mathrm{ham}(\tilde{x}\oplus\tilde{k}')b)+(a+\mathrm{ham}(\tilde{x}\oplus\tilde{k})b)}{2}\right)^2}{2(\sigma/\sqrt{2})^2}} \mathrm{e}^{-\frac{\left((a+\mathrm{ham}(\tilde{x}\oplus\tilde{k}')b)-(a+\mathrm{ham}(\tilde{x}\oplus\tilde{k})b)\right)^2}{4\sigma^2}}\,\mathrm{d}y \\
&= \frac{1}{2\sqrt{\pi}\sigma}\mathrm{e}^{-\frac{\left(\mathrm{ham}(\tilde{x}\oplus\tilde{k}')-\mathrm{ham}(\tilde{x}\oplus\tilde{k})\right)^2}{4(\sigma/b)^2}}.
\end{aligned}
\tag{12}
$$

Equation (12) confirms the intuition that the expectation is maximal if $\tilde{k}'=\tilde{k}$, and that it is the smaller the more the assumed Hamming weight $\mathrm{ham}(\tilde{x}\oplus\tilde{k}')$ differs from the correct Hamming weight $\mathrm{ham}(\tilde{x}\oplus\tilde{k}')$. We note that $G=\{0,1\}^d$, equipped with $\oplus$ (bitwise XOR-operation), is an Abelian group. In particular, $\mathcal{C}(0)$ is a subgroup of $G$ with index 2. If $\tilde{x}\in\mathcal{C}(0)$, then $\mathcal{C}(i)\oplus\tilde{x}=\mathcal{C}(i)$ for $i=0,1$, whereas $\mathcal{C}(i)\oplus\tilde{x}=\mathcal{C}(1-i)$ if $\tilde{x}\in\mathcal{C}(1)$. If we assume that the shared plaintexts are uniformly distributed on $\{0,1\}^d$, then (12), Fubini's Theorem and the above considerations simplify (8) (with $\tilde{x}$ in place of $x$) to

$$
\begin{aligned}
A(k'\mid k) &= \sum_{\tilde{x}\in\{0,1\}^d}\sum_{\tilde{k}'\in\mathcal{C}(k')}\sum_{\tilde{k}\in\mathcal{C}(k)} \frac{1}{2\sqrt{\pi}\sigma}\mathrm{e}^{-\frac{\left(\mathrm{ham}(\tilde{x}\oplus\tilde{k}')-\mathrm{ham}(\tilde{x}\oplus\tilde{k})\right)^2}{4(\sigma/b)^2}} \\
&= 2^{d-1}\left(\sum_{\tilde{k}'\in\mathcal{C}(k')}\sum_{\tilde{k}\in\mathcal{C}(k)} \frac{1}{2\sqrt{\pi}\sigma}\mathrm{e}^{-\frac{\left(\mathrm{ham}(\tilde{k}')-\mathrm{ham}(\tilde{k})\right)^2}{4(\sigma/b)^2}}\right. \\
&\qquad\left. + \sum_{\tilde{k}'\in\mathcal{C}(1-k')}\sum_{\tilde{k}\in\mathcal{C}(1-k)} \frac{1}{2\sqrt{\pi}\sigma}\mathrm{e}^{-\frac{\left(\mathrm{ham}(\tilde{k}')-\mathrm{ham}(\tilde{k})\right)^2}{4(\sigma/b)^2}}\right).
\end{aligned}
\tag{13}
$$

Likewise, (13) also applies when $x$ is not uniformly distributed on $\{0,1\}^d$ but uniformly distributed on $\{0,1\}$ with $\tilde{x}=(x,0\dots,0)$, the case which corresponds to the Clyde cipher. In this case, the factor $2^{d-1}$ is replaced by 1, and $\tilde{x}\in\{0,1\}^d$ in the outer sum reads $x\in\{0,1\}$ (also in (8)). Note that (13) does not depend on $\tilde{x}$. Furthermore, also (14) remains valid with smaller constant $c$.

By (13) it suffices to verify the sufficient condition (9) for $(k,k')\in\{(0,0),(0,1)\}$. Obviously, in $\mathcal{C}(0)$ there exist $\binom{d}{2u}$ elements with Hamming weight $2u$ (for $0\le 2u\le d$), while $\mathcal{C}(1)$ contains $\binom{d}{2v+1}$ elements with Hamming weight $2v{+}1$ (for $0\le 2v{+}1\le d$). This observation allows to further simplify (13) to

$$
\begin{aligned}
A(0\mid 0) &= c\left(\sum_{u=0}^{\lfloor\frac{d}{2}\rfloor}\sum_{v=0}^{\lfloor\frac{d}{2}\rfloor}\binom{d}{2u}\binom{d}{2v}z_0^{(2u-2v)^2} + \sum_{u=0}^{\lfloor\frac{d-1}{2}\rfloor}\sum_{v=0}^{\lfloor\lfloor\frac{d-1}{2}\rfloor}\binom{d}{2u+1}\binom{d}{2v+1}z_0^{(2u-2v)^2}\right) \\
A(1\mid 0) &= c\left(\sum_{u=0}^{\lfloor\frac{d-1}{2}\rfloor}\sum_{v=0}^{\lfloor\frac{d}{2}\rfloor}\binom{d}{2u+1}\binom{d}{2v}z_0^{(2u+1-2v)^2} + \sum_{u=0}^{\lfloor\frac{d}{2}\rfloor}\sum_{v=0}^{\lfloor\lfloor\frac{d-1}{2}\rfloor}\binom{d}{2u}\binom{d}{2v+1}z_0^{(2u-2v-1)^2}\right),
\end{aligned}
\tag{14}
$$

with $c=\frac{2^{d-1}}{2\sqrt{\pi}\sigma}>0$ and $z_0=\mathrm{e}^{-\frac{1}{4(\sigma/b)^2}}\in(0,1)$.

For the special case $d=3$, careful computations yield

$$A(0\mid 0)=2c\left(10+6z_0^4\right) \qquad \text{and} \qquad A(1\mid 0)=2c\left(15z_0+z_0^9\right).$$

It remains to show that $A(0 \mid 0) - A(1 \mid 0) > 0$ (sufficient condition (9)). Let

$$p(z) \coloneqq 10 - 15z + 6z^4 - z^9,$$

so that $A(0 \mid 0) - A(1 \mid 0) > 0$ is equivalent to $p(z_0) > 0$. It is $p(z) > 0$ for $z \in (0,1)$: We have $p'(z) = -15 + 24z^3 - 9z^8$ and $p''(z) = 72z^2 - 72z^7$, so in particular $p(0) = 10$, $p(1) = 0$, $p'(0) = -15$, $p'(1) = 0$ and $p''(z) > 0$ for $z \in (0,1)$. Thus $p'(z) < 0$ for $z \in (0,1)$, which proves the claim. Hence for $d = 3$, condition (9) is fulfilled. Similarly,

$$A^*(0 \mid 0) = c^* \cdot 1 \qquad \text{and} \qquad A^*(1 \mid 0) = c^* z_0,$$

where $c^* = \frac{1}{2\sqrt{\pi}\sigma} > 0$ and $z_0 = \mathrm{e}^{-\frac{1}{4(\sigma/b)^2}} \in (0,1)$, and thus $A^*(0 \mid 0) > A^*(1 \mid 0)$.
In summary: For $d = 3$, the sufficient conditions (9) and (11) are fulfilled so that both decision rules (7) and (10) lead to successful attacks.

## 5.2 Numerical Results

Next, we show some numerical results of the stochastic approach and discuss its advantages and shortcomings. In particular, we have a closer look at the estimated basis coefficients and the information they contain, which helps understanding why attacking different $S$-boxes is so differently difficult. We focus on $d = 3$ shares here, substract a global mean trace before the estimation and use only those operations that can be exploited without any masking bits, namely the key loading, the plaintext and tweak addition and the ISW-multiplication in the first two steps of the $S$-box computation, see also Remark 4. This yields in total 50 POIs that are chosen manually by inspecting the evolution of the estimated coefficients for $S$-box 17 in the interval in which the respective operation takes place. Indeed, for the selected $S$-box there is always a sharp peak in the signal that allows to take the corresponding time point as POI. As we know that all $s = 32$ $S$-boxes are processed in parallel, the same POIs can be taken for all other $S$-boxes as well. Figure 9 exemplarily shows the evolution of the $4 \cdot d = 12$ estimated coefficients for the key loading (left column) and the ISW-multiplications $a_i \odot b_i$ (middle column) respective $a_i \odot b_j$ (right column) in case of the “easy” $S$-box 17 (top row), an “medium” $S$-box 23 (middle row) and a “difficult” $S$-box 0 (bottom row). Each subfigure depicts the evolution of the estimated values of the coefficients in front of the different basis functions, plotted over the time range in which the respective operations take place. Already here the coefficients indicate that the different $S$-boxes are differently difficult to attack, as the coefficients of the “easy” $S$-box 17 are very clear, while the ones of the harder $S$-boxes are much noisier. In particular for $S$-box 17 one sees a sharp peak for each basis function, which allows to select appropriate POIs simply by visual inspection. Also, depending on the exploited operation, the order of magnitude of the coefficients for the different $S$-boxes varies considerably, the coefficients for $S$-box 17 are up to five times as large as those for e.g. $S$-box 0.
To further illustrate the different difficulty levels, we display in Figure 11 the evolution of the coefficient corresponding to a single key bit if all 32 $S$-boxes are estimated simultaneously, again plotted over the time range in which the respective operations take place. In accordance with the observations in the neural network approach, see also Figure 3, the easiest $S$-box 17 shows the highest peak, while the medium $S$-boxes 20, 23 or 26 already yield significantly lower peaks (approximately one half of the maximal peak), which are however still clearly distinguishable from the other, rather noisy signals of the remaining $S$-boxes whose height is only one sixth compared to the maximal height. These observations are qualitatively similar in case of the ISW-multiplications.
Next, we examined how many traces are needed to identify the correct (unshared) key. In case of $S$-box 17, these are approximately 50 traces when avoiding operations that

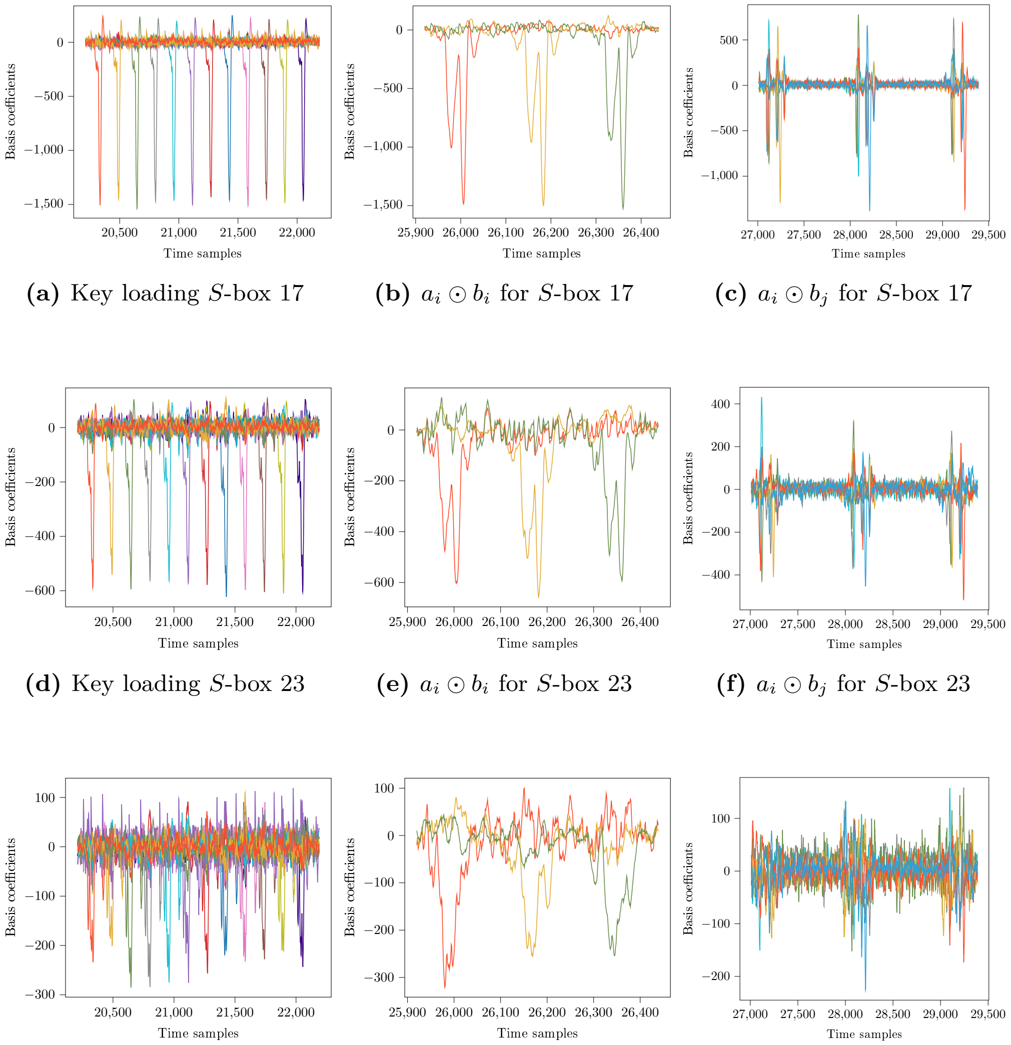

**(a)** Key loading $S$-box 17

**(b)** $a_i \odot b_i$ for $S$-box 17

**(c)** $a_i \odot b_j$ for $S$-box 17

**(d)** Key loading $S$-box 23

**(e)** $a_i \odot b_i$ for $S$-box 23

**(f)** $a_i \odot b_j$ for $S$-box 23

**(g)** Key loading $S$-box 0

**(h)** $a_i \odot b_i$ for $S$-box 0

**(i)** $a_i \odot b_j$ for $S$-box 0

**Figure 9:** Estimation of the basis coefficients for different operations and $S$-boxes. Each subfigure depicts the evolution of the estimated values of the coefficients in front of the different basis functions, plotted over the time range in which the respective operations take place. Please note the different scale of the $y$-axis.

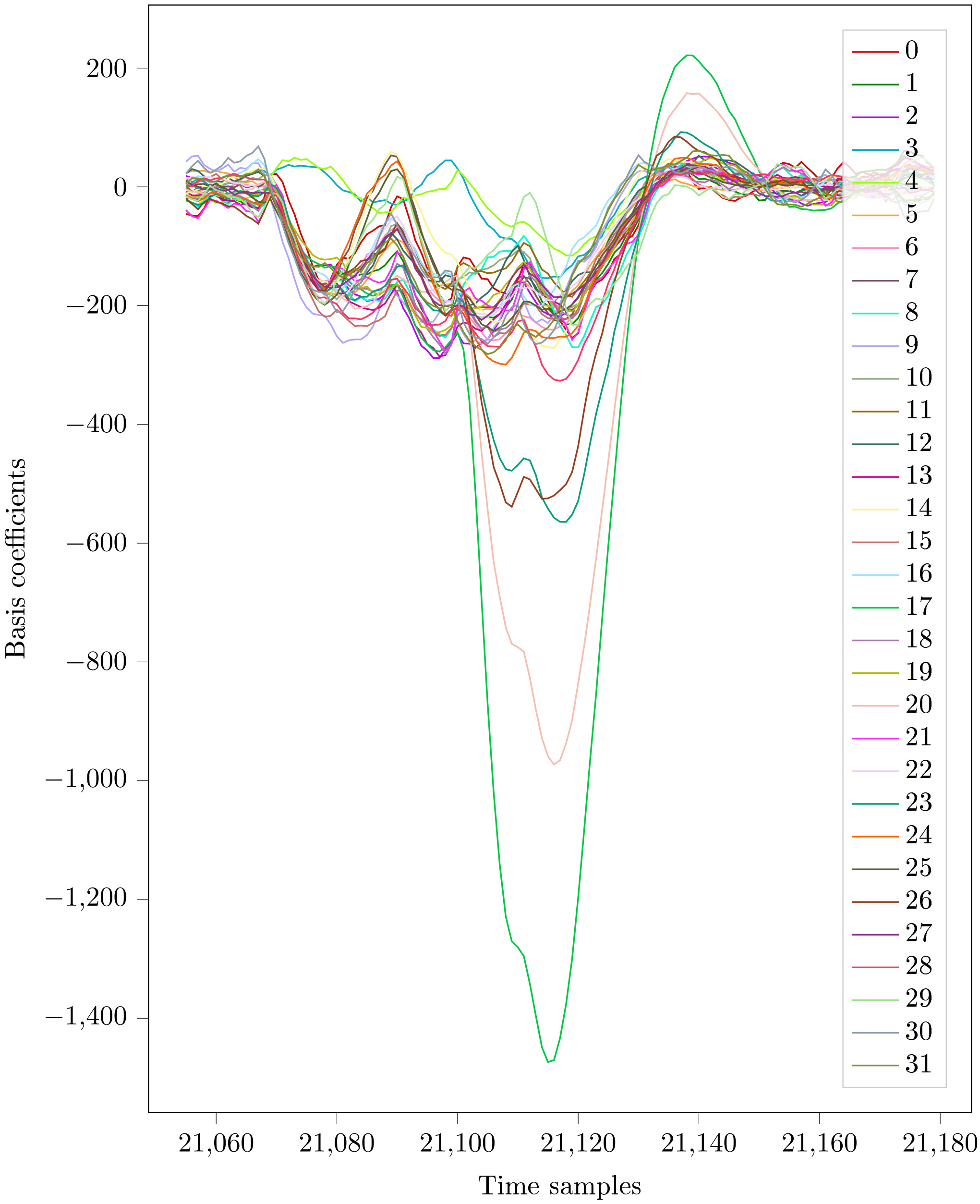

**Figure 11:** Estimation of the basis coefficients for different operations and all $S$-boxes simultaneously. The figure depicts the evolution of the coefficient corresponding to a single key bit of the keyloading if all 32 $S$-boxes are estimated simultaneously, plotted over the time range in which the operations takes place.

involve masking bits. It turned out that including masking bits does not yield significantly better results, but leads to a much higher numerical effort in the attack phase. This might be explained by the observation that already the key loading and the plaintext addition involve all unknown key bits and that their estimated coefficients are higher and clearer as in case of the operations in the context of the ISW-multiplication.

*Remark* 6 (Alternate attack methods). (i) High-dimensional bases for the particular time instants $t_j$ did not yield better results than the bases we used (c.f. Subsection 5.1.1), neither did a PCA for dimension reduction.

(ii) "Full" template attacks (i.e., template attacks that do not apply assumptions on the leakage) can be viewed as a special case of the stochastic approach using the full basis. When attacking a single $S$-box $2^{4d}$ ($= 2^{12}$ for $d = 3$) different shared subkeys and $2^4$ different tweak bits can occur so that $2^{12+4} = 2^{16}$ densities need to be estimated, neglecting possible masking bits. In average, only $200,000/2^{16} \approx 3$ power traces would be available for the estimation of 50-dimensional densities (we exploited 50 time instants). The dimension cannot substantially be reduced (without loss of information) because for $d = 3$, we exploit 12 (key loading) +12 (state initialization[6]) $+2 \cdot 4$ (tweak and plaintext addition, each on the first slice) $+2 \cdot 3$ (first two ISW multiplications $a_i \odot b_i$) $+2 \cdot 6$ (first two ISW multiplications $a_i \odot b_j$ $= 50$ operations which take place at different times. Thus full template attacks (exploiting all operations considered by the stochastic approach) are not practical in this scenario. Experiments with templates we conducted on fewer POIs (either selected manually as for the stochastic approach or by estimating the signal-to-noise ratio) were not succesful.

(iii) In practice, often "model-based" template attacks are used which apply simple leakage model assumptions (e.g., Hamming weight model or Hamming distance model) to drastically reduce the number of densities to be estimated. In the given scenario for different time instants, distinct leakage models apply (c.f. Subsection 5.1.1) so that a "simple" joint leakage model should hardly exist. In particular, there is no reason to assume that model-based template attacks are more effective than the applied stochastic approach.

(iv) The stochastic approach allows to split the calculation of high-dimensional densities into the independent estimation of several one-dimensional leakage functions (with individual leakage models) and of one covariance matrix. This leads to an efficient exploitation of the leakage. Below, a further advantage of the stochastic approach will be exploited, namely the possibility of gaining insights into the nature of the leakage.

Contrary to the deep learning based approach, the attack phase does not succeed for the difficult $S$-boxes, even when taking a high number of traces. This is most likely due to the fact that already the estimation of the coefficients yield rather poor results.

The leakage of the "easy" $S$-box 17 is very large, allowing a successful attack on subkey $k_{17}$. Unfortunately, its large leakage spoils the sigma-to-noise ratio of the other $S$-boxes. The signal-to-noise ratio quantifies the impact of small and large $\beta$-coefficients on the overall leakage. For the moment, we define $\vec{x} = (x_0, \ldots, x_{31})$, $\vec{z} = (z_0, \ldots, z_{31})$, and $\vec{\tilde{k}} = (\tilde{k}_0, \ldots, \tilde{k}_{31})$, and we assume that the power consumptions of all $S$-boxes are independent. This justifies to extend equation (4) from a single to all $S$-boxes by

$$I_t(\vec{x}, \vec{z}, \vec{\tilde{k}}) = \sum_{j=0}^{31} h_{t(j)}(x_j, z_j, \tilde{k}_j) + R_t^*.$$

[6] The shared state is initialized with the shared key so that the leakage of the sensitive key can actually be exploited twice.

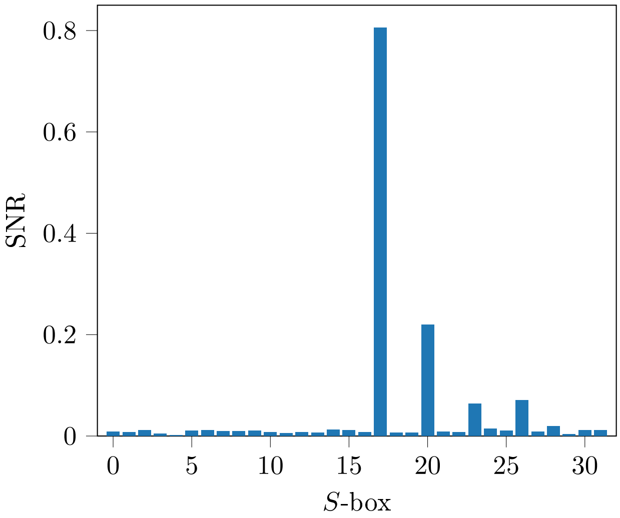

**Figure 12:** Estimation of the signal-to-noise ratio of the different $S$-boxes for the key loading operation.

The random variable $R_t^*$ summarizes the (centered) noise at time $t$ that does not originate from any of the 32 $S$-box operations but from further operations that take place at the same time. We interpret the values $x_0, \dots, x_{31}$ and $z_0, \dots, z_{31}$ as realizations of independent random variables $X_0, \dots, X_{31}$, $Z_0, \dots, Z_{31}$, so that

$$\operatorname{Var}\left(I_t(\vec{X}, \vec{Z}, \vec{\tilde{k}})\right) = \sum_{j=0}^{31} \operatorname{Var}_{X_j, Z_j}\left(h_{t(j)}(X_j, Z_j, \tilde{k}_j)\right) + \operatorname{Var}\left(R_t^*\right).$$

The term $\operatorname{Var}_{X_j,Z_j}(\cdot,\cdot,\cdot)$ quantifies the "algorithmic noise" that depends on $X_j, Z_j$ and $\tilde{k}_j$. Given a fixed shared key $\vec{\tilde{k}}$, it depends on the signal-to-noise ratio

$$\operatorname{SNR}(r) := \frac{\operatorname{Var}_{X_r, Z_r}\left(h_{t(r)}(X_r, Z_r, \tilde{k}_r)\right)}{\sum_{j=0,\dots,31; j \neq r} \operatorname{Var}_{X_j, Z_j}\left(h_{t(j)}(X_j, Z_j, \tilde{k}_j)\right) + \operatorname{Var}\left(R_t^*\right)}$$

whether an $S$-Box $r$ is "easy" or "difficult".
If $g_{(j),0,t,\tilde{k}_j} = 1, g_{(j),1,t,\tilde{k}_j}, \dots, g_{(j),u-1,t,\tilde{k}_j}$ denotes an orthonormal basis for $S$-box $j$, the computation of the algorithmic variance of $S$-box $j$ simplifies to

$$\operatorname{Var}_{X_j, Z_j}\left(h_{t(j)}(X_j, Z_j, \tilde{k}_j)\right) \approx \sum_{\tau=1}^{u-1} \beta^2_{(j),\tau,t;\tilde{k}_j} \approx \sum_{\tau=1}^{u-1} \tilde{\beta}^2_{(j),\tau,t;\tilde{k}_j}.$$

Figure 12 shows the estimated signal-to-noise ratio of the different $S$-boxes for the key loading operation. The corresponding figures of the other operations look qualitatively similar.

## 5.3 Leakage Assessment

The implementation at hand is especially protected against side-channel attacks. Nevertheless, with our neural network-based approach it is possible to extract enough information to reveal the secret key, and in the aftermath of the contest we had a closer look at the parts of the implementation that are actually leaking sensitive information.

By its design it is evident which operations of the algorithm the stochastic approach exploits, as these are directly reflected in the choice of the basis functions. For the neural network approach, however, it is less clear which information the network uses, since it is fed with the whole (subsampled) traces and performs the selection of relevant points on its own. At the same time, this illustrates one of the major advantages of neural network-based approaches, as they do not require the preselection of points of interest, but find them of their own.

We did different experiments to find out which points in the trace are important for our neural network based leakage extractor. All of them were run on the 3-share data set, as we did not expect substantially different phenomena to appear for the higher targets. We did, however, not test this assumption, but leave it for future research. We tried the following techniques:

- First, we subdivided our 62,500 point into 625 windows, each of which consisting of 100 points, and compared the predicted bit probabilities for the shared state before and after zeroizing each window, averaging results over a small set of traces.
- We calculated the gradient of the predictor as a function of the input trace for a subset of input traces in our data set.

In both experiments, we assumed that points that are of interest to the neural network would show up as points in which the influence of small changes to the trace on the prediction output is high. Both experiments yielded qualitatively similar results, so we only describe the results of the window-wise zeroization experiment in more details.

**Methods** We selected 200 traces from the data set Fkey_Sw3_K1_1000_0, sent them through our predictor, and converted the scattershot predictions into predictions of single key bits. We then zeroized each of our 625 windows in turn, ran the same prediction using the altered trace, and finally calculated the mean squared error of the new prediction with respect to the prediction obtained from the unaltered trace.

**Results** The main active region for all traces was found to be between data points 35,000 and 60,000, with smaller and less significant active regions also at the very beginning of the trace for some $S$-boxes. Within that very broad active region, large differences in signal attribution were observed between different $S$-boxes. Figure 13 shows the relevant profile for the $S$-boxes 17, 0 and 22. It is worth noting here that the prediction of the particularly difficult $S$-box 22 draws on some regions of the trace that are not used at all for the other two $S$-boxes. Matching the operations of the algorithm with the shape of the trace and the time points the first two active regions around time point 38,000 and 43,000 are during the $S$-box computation, more precisely they correspond to the ISW-multiplications $\big(y[1,\cdot] \odot x[3,\cdot]\big) \oplus x[0,\cdot]$ and $y[2,\cdot] = \big(y[0,\cdot] \odot y[1,\cdot]\big)$ (see equation (1)) after the mask refreshing. The very active region after point 48,000 is during the computation of the $L$-box, which is rather surprising and seems a bit odd since the network actually aims at predicting the $S$-box output. Furthermore, it might serve as an explanation why the AI-based approach considerably outperforms the stochastic approach (and any other classical approach we tried such as templates), since these approaches cannot exploit the $L$-box computation acting on rows of the Clyde-state instead of columns. This is mainly due to numerical reasons, in particular the huge amount of masking bits and the fresh randomness caused by the mask refreshing. The stochastic approach yet helped us to understand why attacks on different $S$-boxes are so differently efficient and allowed to quantify this knowledge.

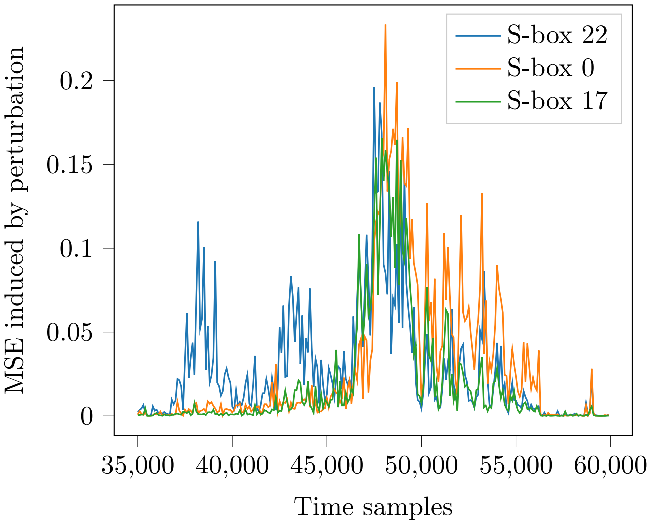

**Figure 13:** Results of our main leakage attribution experiment for our deep neural network. We divided the input traces for the 3-share challenge into 625 windows 100 data points in length and recorded the mean squared error induced in the state bit predictions by zeroizing each window input (i.e. predictions were generated before and after zeroizing the window and the mean squared difference between these two vectors was plotted), where we show the results for three selected $S$-boxes.

## 6 Conclusion and Future Work

In this paper we presented our deep learning-based solution to the CHES 2020 challenge and gave further insights into certain aspects of our approach, in particular the scattershot encoding.

Furthermore, we provided and analyzed an alternative, "classical" method, namely the stochastic approach. Compared to previous works, both the AI-method (in form of the scattershot encoding) as well as the stochastic approach (in form of the key extraction phase) had to be adapted to cope with the masked cipher encountered in the contest, where the randomly chosen shared states make the combination of leakage information across different traces much more difficult compared to an unshared setting.

Our results show that a deep learning based attack using only a limited amount of information about the implementation can defeat a software implementation logically protected by a higher-order masking of the cipher state without much manual intervention. To train our attack, we only need to be able to calculate the shared internal state after the first $S$-box calculation; while we do need to know the masking randomness of the training traces, we do not need to analyze the details of the implementation beyond the logic that allows us to compute that shared internal state. Our results show that the choice of the encoding of the target values can have a large impact on network convergence. Furthermore, our work shows that adversaries can break cryptographic implementations like the one used in this challenge in a largely automated way; however, it is also clear that simply increasing the order of the masking countermeasure would eventually protect against such attacks, as usual at the cost of computational resources and performance.

However, our results also show that explaining the leakage found by such methods is not always easy: we do, for instance, not have a good explanation from first principles yet for the massive difference in the magnitude of leakage observed for different $S$-boxes. In addition, it can be difficult to distinguish logical problems of leakage extraction from the lack of leakage: this point is driven home especially by our experiments to better understand the effect of the scattershot encoding using a completely synthetic problem. Finally, our research also shows that much remains to be discovered in a wide variety of areas around ML-based side-channel attacks: pre-processing, data representation, network architectures and post-processing model outputs are all less well understood for side-channel analysis than in more standard application domains of ML methods such as signal and in particular image processing tasks.

## References

[1] G. Barthe, S. Belaïd, F. Dupressoir, P.-A. Fouque, B. Grégoire, F.-X. Standaert, and P.-Y. Strub. Improved parallel mask refreshing algorithms: generic solutions with parametrized non-interference and automated optimizations. *Journal of Cryptographic Engineering*, 10:1–10, 2019.

[2] G. Barthe, F. Dupressoir, S. Faust, B. Grégoire, F.-X. Standaert, and P.-Y. Strub. Parallel implementations of masking schemes and the bounded moment leakage model. Cryptology ePrint Archive, Report 2016/912, 2016. https://eprint.iacr.org/2016/912.pdf.

[3] C. Beierle, J. Jean, S. Kölbl, G. Leander, A. Moradi, T. Peyrin, Y. Sasaki, P. Sasdrich, and S. M. Sim. The SKINNY family of block ciphers and its low-latency variant MANTIS. In *Annual International Cryptology Conference*, pages 123–153. Springer, 2016.

[4] D. Bellizia, F. Berti, O. Bronchain, G. Cassiers, S. Duval, C. Guo, G. Leander, G. Leurent, I. Levi, C. Momin, et al. Spook: Sponge-based leakage-resistant authenticated encryption with a masked tweakable block cipher. *IACR Transactions on Symmetric Cryptology*, 2020.

[5] D. Bellizia, O. Bronchain, G. Cassiers, C. Momin, F. Standaert, and B. Udvarhelyi. CHES 2020 Spook Side-Channel Analysis Capture the Flag Challenge (Spook SCA CTF), 2020. https://ctf.spook.dev/.

[6] O. Bronchain and F. Standaert. Breaking masked implementations with many shares on 32-bit software platforms or When the security order does not matter. *IACR Transactions on Cryptographic Hardware and Embedded Systems*, 2021(3):202–234, 2021.

[7] G. Cassiers, B. Grégoire, I. Levi, and F.-X. Standaert. Hardware private circuits: From trivial composition to full verification. Cryptology ePrint Archive, Report 2020/185, 2020. https://eprint.iacr.org/2020/185.

[8] M. Cordts, M. Omran, S. Ramos, T. Rehfeld, M. Enzweiler, R. Benenson, U. Franke, S. Roth, and B. Schiele. The cityscapes dataset for semantic urban scene understanding. In *Proceedings of the IEEE conference on computer vision and pattern recognition*, pages 3213–3223, 2016.

[9] L. Fei-Fei, J. Deng, and K. Li. ImageNet: Constructing a large-scale image database. *Journal of vision*, 9(8):1037–1037, 2009.

[10] C. Glowacz, V. Grosso, R. Poussier, J. Schüth, and F.-X. Standaert. Simpler and more efficient rank estimation for side-channel security assessment. In *International Workshop on Fast Software Encryption*, pages 117–129. Springer, 2015.

[11] A. Gohr, S. Jacob, and W. Schindler. Subsampling and knowledge distillation on adversarial examples: New techniques for deep learning based side channel evaluations. In *Selected Areas in Cryptography*, volume 12804 of *Lecture Notes in Computer Science*, pages 567–592. Springer, 2020.

[12] D. Goudarzi and M. Rivain. How fast can higher-order masking be in software? In J.-S. Coron and J. B. Nielsen, editors, *Advances in Cryptology*, pages 567–597, Cham, 2017. Springer International Publishing.

[13] V. Grosso, G. Leurent, F.-X. Standaert, and K. Varıcı. LS-designs: Bitslice encryption for efficient masked software implementations. In *International Workshop on Fast Software Encryption*, pages 18–37. Springer, 2014.

[14] V. Grosso, G. Leurent, F.-X. Standaert, K. Varici, F. Durvaux, L. Gaspar, and S. Kerckhof. SCREAM & iSCREAM side-channel resistant authenticated encryption with masking. *Submission to CAESAR*, 2014. https://competitions.cr.yp.to/round2/screamv3.pdf.

[15] Y. Ishai, A. Sahai, and D. Wagner. Private circuits: Securing hardware against probing attacks. In *Annual International Cryptology Conference*, pages 463–481. Springer, 2003.

[16] J. Kim, S. Picek, A. Heuser, S. Bhasin, and A. Hanjalic. Make some noise. Unleashing the power of convolutional neural networks for profiled side-channel analysis. *IACR Transactions on Cryptographic Hardware and Embedded Systems*, 2019(3):148–179, 2019.

[17] G. M. Kurtzer, V. Sochat, and M. W. Bauer. Singularity: Scientific containers for mobility of compute. *PLOS ONE*, 12(5):1–20, 2017.

[18] L. Masure, N. Belleville, E. Cagli, M.-A. Cornélie, D. Couroussé, C. Dumas, and L. Maingault. Deep learning side-channel analysis on large-scale traces. In *European Symposium on Research in Computer Security*, pages 440–460. Springer, 2020.

[19] National Institute of Standards and Technology (NIST). Lightweight cryptography standardization process, August 2018. https://csrc.nist.gov/Projects/lightweight-cryptography.

[20] S. Picek, A. Heuser, A. Jovic, S. Bhasin, and F. Regazzoni. The curse of class imbalance and conflicting metrics with machine learning for side-channel evaluations. *IACR Transactions on Cryptographic Hardware and Embedded Systems*, 2018(1):209–237, 2018.

[21] S. Picek, G. Perin, L. Mariot, L. Wu, and L. Batina. SoK: Deep learning-based physical side-channel analysis. Cryptology ePrint Archive, Report 2021/1092, 2021. https://ia.cr/2021/1092.

[22] W. Schindler, K. Lemke, and C. Paar. A stochastic model for differential side channel cryptanalysis. In J. R. Rao and B. Sunar, editors, *Cryptographic Hardware and Embedded Systems*, pages 30–46, Berlin, Heidelberg, 2005. Springer Berlin Heidelberg.

[23] L. Wu, G. Perin, and S. Picek. The best of two worlds: Deep learning-assisted template attack. Cryptology ePrint Archive, Report 2021/959, 2021. https://ia.cr/2021/959.

[24] L. Wu, G. Perin, and S. Picek. On the evaluation of deep learning-based side-channel analysis. In *International Workshop on Constructive Side-Channel Analysis and Secure Design*, pages 49–71. Springer, 2022.

[25] G. Zaid, L. Bossuet, M. Carbone, A. Habrard, and A. Venelli. Conditional variational autoencoder based on stochastic attack. Cryptology ePrint Archive, Report 2022/232, 2022. https://ia.cr/2022/232.

[26] G. Zaid, L. Bossuet, F. Dassance, A. Habrard, and A. Venelli. Ranking loss: Maximizing the success rate in deep learning side-channel analysis. *IACR Transactions on Cryptographic Hardware and Embedded Systems*, pages 25–55, 2021.